



Assessment of Earthquake Activity of a Rift-Bounding Fault, Northwest of Gulf of Suez, Egypt



Abd-elhadi S. A. Mohammad¹, Karim Abdelmalik¹, Sherif M. Elhady² and Ali M. A. Abd-Allah¹

¹Geology Department, Faculty of Science, Ain Shams University, Cairo, Egypt

²Seismology Department, National research Institute of astronomy and geophysics, Egypt

Ongoing tectonic activity—originally responsible for the development of a rift-bounding fault system in the northwestern Gulf of Suez, Egypt—has prompted a preliminary assessment of related seismic events. The study focuses on several urbanized sites along the western coastline, where recent surface fractures were documented and analysed to explore their connection to ongoing seismicity. It is an initial attempt to apply TENSOR stress inversion techniques—such as PBT and right-dihedral methods—were applied to field-measured fracture data that were systematically collected from six key sites. The analysis generated reduced stress tensors, rose diagrams, Mohr circles, and stereographic projections, revealing localized stress regimes across the region, from which the mean stress regime acting upon the entire region was retrieved. While most sites displayed pure or axial extensional stress fields, transtensional regimes were identified in specific cases. The spatial correlation between recent fracture orientations and the traces of pre-existing deep-seated faults revealed dominant E–W to NNW–SSE trends, consistent with the stress fields associated with Miocene Gulf of Suez rifting. However, notable ENE–WSW fracture patterns observed at Banzeenah and Porto sites suggest the presence of additional localized tectonic influences. Overall, those integrated approaches highlight the continued reactivation of pre-existing rift-related structures and their role in present-day seismic deformation along the western margin of the Gulf of Suez.

Keywords: Neo-tectonic analysis, Stress tensor, Post-seismic deformation, Western Gulf of Suez coasts.

1. Introduction

The Northern Gulf of Suez seismogenic source (EG-17) (Sawires et al., 2015) (Figure 1) is recognized as a seismically active region due to its geological structure, which forms part of the Galala structural province (Husseini and Abd-Allah, 2001). The area's seismicity results from ongoing tectonic activity, resulting from the convergence between the African and Eurasian plates, extensional forces in the Gulf of Suez, and strike-slip motion along the Gulf of Aqaba–Dead Sea fault zone (Sawires et al., 2015).

This research focuses on examining newly developed fractures in selected urbanized areas located along the western shores of the northern Gulf of Suez, because its continuous tectonic activity is making it essential to monitor for the potential risks it poses to the area's economic prospects. Fortunately, advancements in earthquake monitoring technologies have enabled more effective observation, and integrating multiple methods provides detailed insights into both

immediate and long-term surface changes resulting from seismic events. The stress analysis of the recent fractures deduces a reduced stress tensor from which orientations of the mean stress axes for the tectonic forces acting upon the entire region can be obtained in order to find a connection between the recent tectonic activity and the last phase of the Miocene Gulf of Suez rifting.

This study presents an initial attempt to evaluate the earthquake activity of a rift-bounding fault system located northwest of the Gulf of Suez, Egypt. The objective is to investigate a correlation between recent surface fractures and ongoing seismicity within the region. To achieve this, we applied TENSOR stress inversion analysis—for the first time in this area—to derive principal stress orientations and investigate their consistency with observed fracture patterns. This approach aims to assess whether the current tectonic regime reflects a continuation of the Miocene Gulf of

*Corresponding author e-mail: shady_abdelhady@sci.asu.edu.eg

Received: 30/05/2025; Accepted: 13/06/2025

DOI: 10.21608/egjg.2025.390447.1116

©2025 National Information and Documentation Center (NIDOC)

Suez rifting and to identify potential zones of reactivation along ancient fault structures.

2. Geological Settings

The southern edge of the Northern Galala Plateau that is delimited by a southeast-dipping positive-inverted fault, signifies the transition boundary with the Araba inversion doubly plunging anticline (Moustafa and Khalil, 2020). Its northwestern limb corresponds to the up-thrown side which occupies a major part of Wadi Araba. Its southeastern limb represents the uplifted side of a northwest-dipping reverse fault, which outlines the northern boundary of the Southern Galala Plateau (Hussein and Abd-Allah, 2001). The structural configuration of the plateau is governed by three primary fault systems (Saada, 2016):

2.1 Set (1) E-W oriented fault set

These faults dip toward the north and define the northern escarpment of the Northern Galala Plateau, including the Northern Galala Fault. This fault system consists of east–west trending listric fault surfaces that are linked by northwest–southeast oriented synthetic normal transfer faults (Hussein and Abd-Allah, 2001).

2.2 Set (2) NW-SE oriented normal faults

These faults constitute the dominant structural framework extending across the Northern Galala Plateau from east to west. They are primarily associated with the Miocene Red Sea–Gulf of Suez rifting but also encompass pre-rift features, such as the Abu Darag Fault. This fault is part of the Rihba shear zone, which has been linked to Precambrian tectonic activity (Younes and McClay, 2002), (Moustafa and Khalil, 2020).

2.3 Set (3) NE-SW oriented faults

Less prevalent fault trends have also been identified (Saada, 2016) such as the southeast-dipping reverse fault that defines the southern scarp of the plateau. Additionally, other minor faults that play a structural role in bounding the Khashm El-Galala high (Abd-Allah, 1993).

The Northern Galala plateau and the western side of the Gulf of Suez had experienced successive tectonic phases, beginning with **Tethyan rifting** as a result of the divergence of the Afro-Arabian plate apart from the Eurasian plates from the Middle–Late Triassic to

Early Cretaceous, which generated ENE–WSW and E–W trending normal faults and lead to the opening of the Neotethys (Moustafa, 2020), (Moustafa and Khalil, 1995). Then a second phase known as **Cretaceous rifting** (Moustafa, 2020). It is believed to have been driven by distant stresses from the opening of the South Atlantic. These forces likely reactivated older fault systems in the region. Evidence of this influence appears in the northern Gulf of Suez, where the Darag Fault—along the eastern margin of the Northern Galala Plateau—shows signs of renewed activity. This deformation extends across the gulf to the reactivated Hammam Faraun Fault, which is aligned with the Rihba Shear Zone described by (Younes and McClay, 2002). The third phase occurred in the Late Cretaceous, and it was known as **Tethyan convergence** leading to the development of inverted structures like the Wadi Araba Anticline (El Shinawi et al., 2022), (Moustafa, 2020). Later, during the Oligocene–Miocene, a fourth phase, known as **Neogene rifting** attributed to extensional tectonics related to Gulf of Suez rifting, formed NE–SW normal faults and contributed to the gulf's opening; e.g (Moustafa and Khalil, 1995) in (El Shinawi et al., 2022) and (Moustafa, 2020). The fifth phase **Dead Sea Transform**, active since the Late Miocene, likely reactivated older NNE-SSW Jurassic faults in a strike-slip movement (Moustafa, 2020). This phase also coincided with volcanic activity, evidenced by basalt flows capping parts of the plateau and valley mouths such as Wadi Umm Qena, Wadi Haroz, and Wadi Noaz (Boukhary et al., 2009).

The stratigraphic sequence of the Northern Galala Plateau and the Gulf of Suez can be broadly categorized into three main divisions. The pre-rift units comprise the Precambrian basement complex and the overlying Phanerozoic sedimentary layers, extending up to Eocene formations. The syn-rift units, especially along the Gulf of Suez such as the Oligocene Abu Zenima Sandstone, the Early Miocene Nukhuk Sandstone and Rudies Shale, Middle Miocene Kareem Sandstone and Evaporites and Balayim Evaporites, followed by Late Miocene Zeit and South Garib Evaporites span the Miocene period, followed by the post-rift deposits, which include Quaternary sediments (Farouk, 2015), (Moustafa and Khalil, 2020).

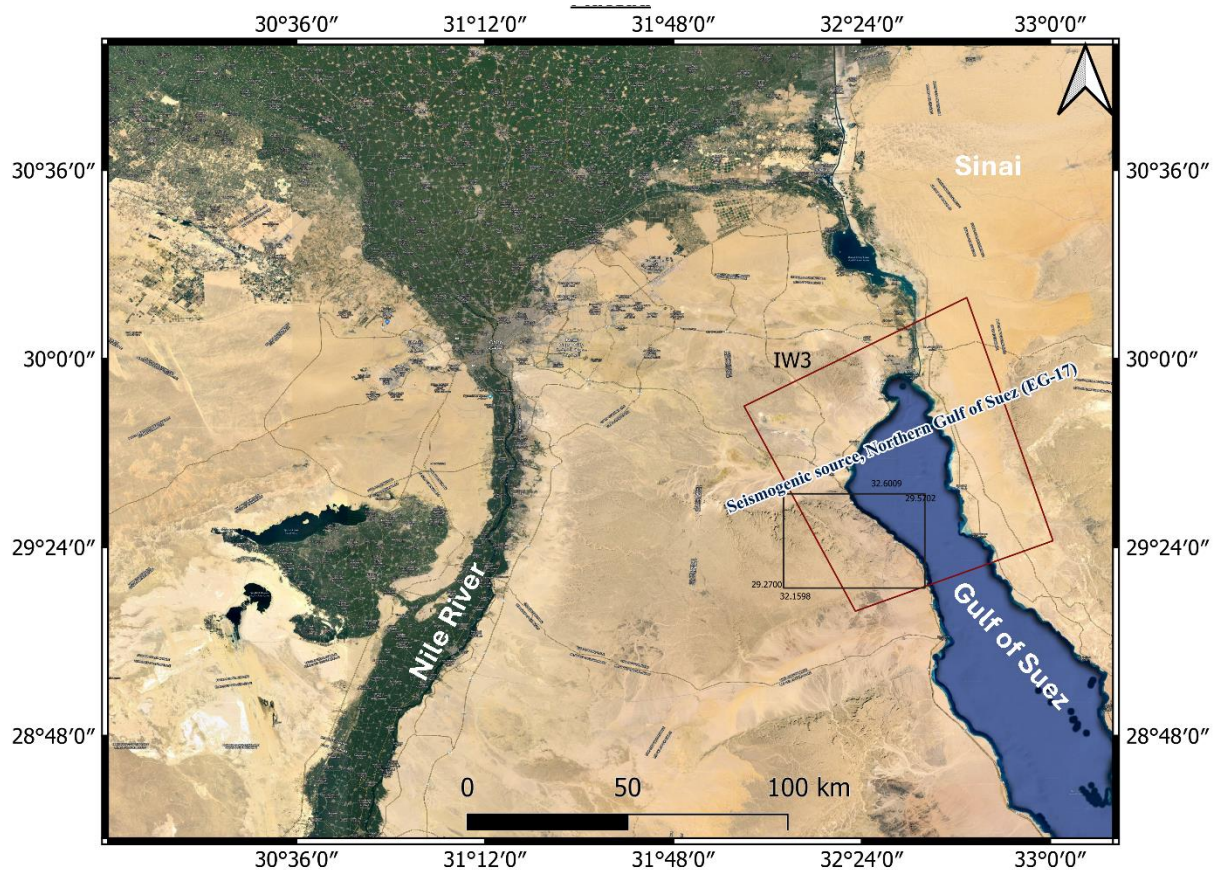


Fig. 1. Base map from Esri showing the boundaries of the study area included inside the Seismogenic source Northern Galala (EG-17) traced from the model after (Sawires et al., 2015).

3. Data and Methodology

3.1 Study area

The study area is primarily focused on urban sites distributed along western coast of the Gulf of Suez, within the coordinates 29°16'12"N to 29°34'12.72"N latitudes. It is accessible from the Hurghada- Al Ismaileya road branches off Cairo- El Sokhna road. The study examines a series of sites distributed along a along the Hurghada- Al Ismaileya road from north to south, namely: Tatweer, Benzeenah, North Porto, Porto, South Porto, and Telal, which were investigated for their recently formed structural features.

3.2 Field-based fracture analysis

Field-based structural measurements were conducted to document the pre-existing of recently formed most prominently extension fractures with measured aperture widths as shown in (Figure 2) in the aforementioned six metropolitan sites under investigation. A field-based survey was conducted,

documenting a variety of fracture sets, predominantly cut through the Quaternary strata. The orientation data collected from each site were analyzed and presented using individual rose diagrams to illustrate the dominant structural trends (Figure 2). The rose diagrams were geospatially projected as superimposed plot on each site to display the orientation patterns of fractures recorded during field measurements at each site, offering insights into the local tectonic regimes (Figure 3). Field-photographs of the discovered fractures (Figure 4) provide qualitative visual evidence of surface deformation consistent with ongoing tectonic activity in the region had an average aperture width of 1-2 centimeters and they exhibit of both fine and more prominent fractures suggest variability in fracture intensity and lithologic control across the sites.

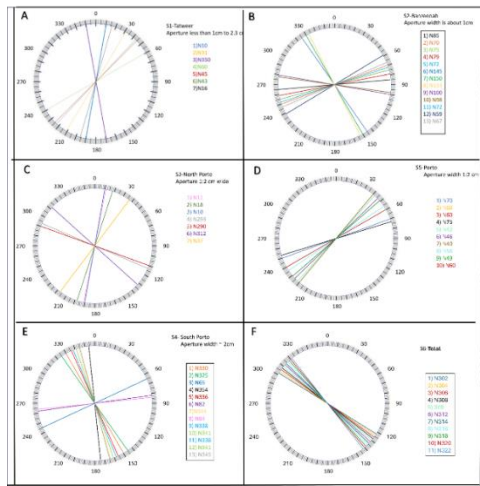


Fig.2. The Orientation-only rose diagram (no magnitude or histogram data) representing the direction of each individual fracture discovered at A) S1-Tatweer, B) S2-Banzeenah, C) S3-North Porto, D) S5-Porto, E) S4-South Porto and F) S6-Telal. The average aperture widths were measured for each fracture set when possible. The column adjacent to each rose diagram lists the exact azimuths of the measured fractures, with each entry color-coded to match its corresponding plot in the diagram.

3.3 Stress Inversion

This **technique** is utilized to reconstruct the mean stress tensor by analyzing a set of faults with known geometries and slip directions (Angelier, 1989), (Pollard et al., 1993). It relies on field-based geological measurements of fault characteristics, (Sippel et al., 2007) specifically:

- the slip direction along the fault,
- the orientation of the fault plane, and
- the sense of slip, typically inferred from features like slickenlines and chatter marks

These structural measurements are then input into specialized software, such as TENSOR developed by (Delvaux, 1993), to determine the reduced stress tensor. This output defines the orientations of the principal stress axes and the stress ratio (R), which is calculated using the following formula (eq.1) (Lisle et al., 2001):

$$R = \left(\frac{\sigma_2 - \sigma_3}{\sigma_1 - \sigma_3} \right) \#(1)$$

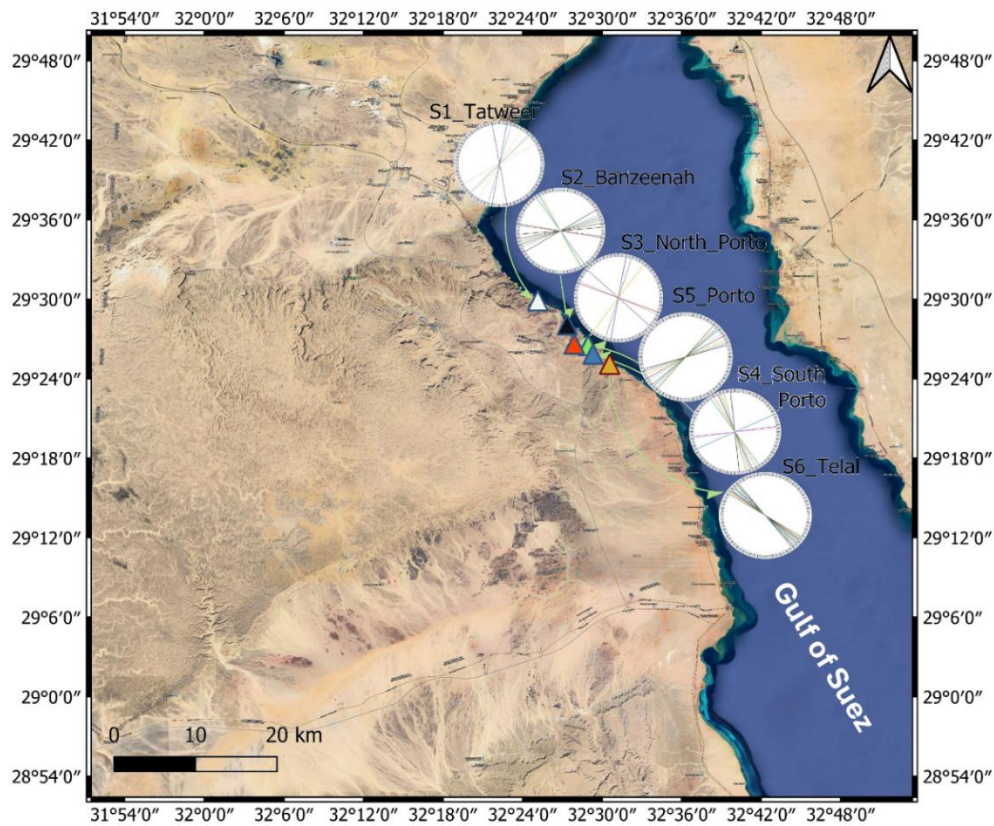


Fig. 3. Base map showing the structural trends plotted into rose diagrams for each investigated site East of the Northern Galala Plateau. Each surveyed site—Tatweer (S1), Banzeenah (S2), North Porto (S3), Porto (S5), South Porto (S4), and Telal (S6)—is represented by a colored triangular symbol.

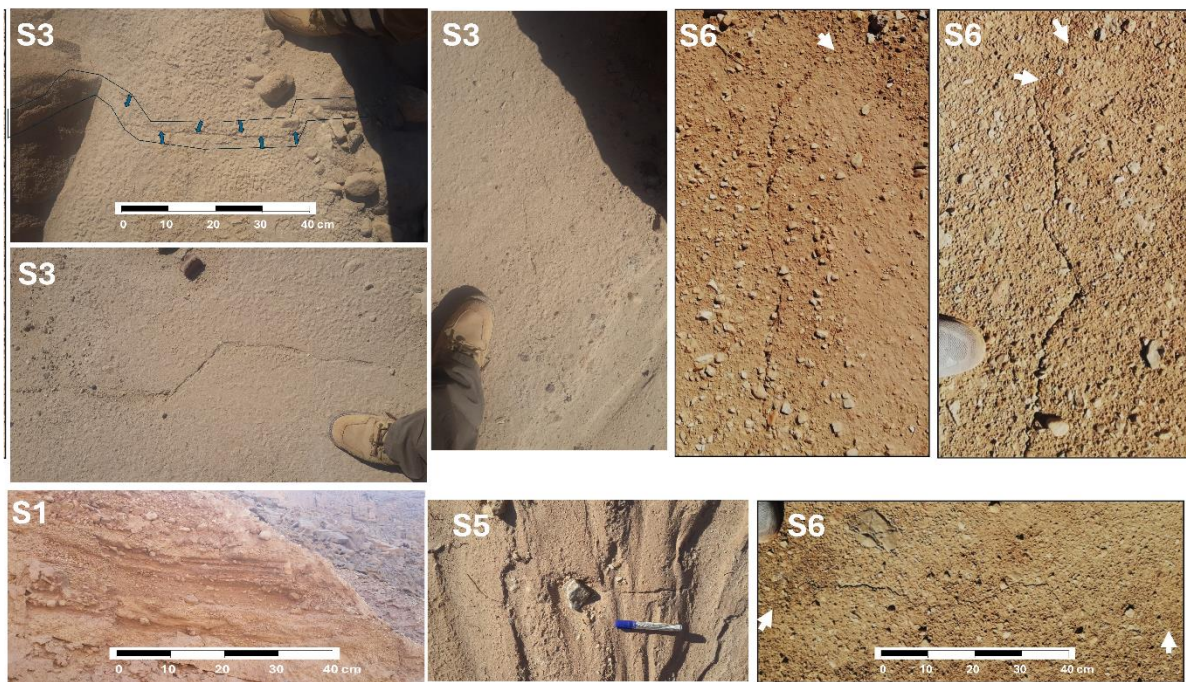


Fig.4. Field photographs showing examples of the measured extension neo-formed fractures. S1-Tatweer, S3 North Porto, S5-Porto and S6-Telal stations stress tensor, characterizing the local stress field at each site.

Tensor processing of the previous input derive five principal axes, which are illustrated using fault-plane solutions similar to those found in earthquake focal mechanism diagrams (Angelier, 1979) (Angelier, 1989). These axes include:

- the slip vector on the primary fault plane,
- the slip vector on the auxiliary plane,
- the P-axis (direction of maximum compressive stress),
- the T-axis (direction of maximum extensional stress), and
- the B-axis (intermediate or null axis).

The universal approaches, **PBT and right dihedral method** are graphical methods whose objective was to retrieve the orientations of the Pressure-Null (neutral)-Tension (PBT) axes and locating dilatational and compressional quadrants around across the fault's vicinity (Mattila, 2015). Although faults may vary in orientation inside a population, nearby sets are generally influenced by the same regional stress field, therefore the graphical methods help constrain the P-dihedral and T-dihedra, allowing the principal stress axes σ_1 and σ_3 to be plotted at their respective centers (Angelier, 1979). Field-measured fractures were categorized into homogenous populations, and each were analyzed independently, with the program performing separate PBT and right-dihedral analyses. Each analysis produced a distinct reduced

3.3.1. PBT method

The pressure and tension axes can be determined by bisecting the compressional and extensional quadrants, with their intersection defining the neutral. The PBT axes correspond to the orthogonal directions of maximum (σ_1), intermediate (σ_2), and minimum (σ_3) (Lisle et al., 2001) (Khattari, 1973). In datasets with multiple fault orientations, the resulting P and T axes form clusters. The principal stress axes σ_1 and σ_3 are then located within their respective quadrants, with their final positions estimated as weighted means within the P, B, and T axis clusters inside the respective quadrants in the Schmedit-Lower stereonet (McKenzie, 1969) (Lisle et al., 2001). Due to the wide variation in fracture trends, Tensor required several rotations of the calculated principal stress axes to determine their optimal orientations. New version of Tensor was capable to run rotational optimization, which is a method developed by (Delvaux and Sperner, 2003), to the results of PBT analysis.

3.3.2. Right-dihedral method

This method involves plotting multiple fault-slip data on a single stereonet, resulting in clusters of P and T axes within overlapping compressional and extensional quadrants. This overlap helps refine the possible orientations of the principal stress axes (Mattila, 2015). The lower-hemisphere Schmidt

stereonet is subdivided into a reference grid, where each point represents a fault-slip measurement (Delvaux & Sperner, 2003). For each fault, the principal stress axes are displayed as blue dots, with their size reflecting relative magnitude (0–100). Averaging these clusters yields the mean orientation of the principal stress axes. That latter were more accurately refined by rotational optimization as well as with the previous PBT method.

Tensor applies both PBT and right-dihedral methods simultaneously yet independently on the input dataset, generating detailed outputs, including a right-dihedral stereonet and optimized stress solutions for each site. To investigate the relationship between the orientations of recent and ancient faults, the previously generated PBT and right-dihedral stereonets were enriched by projecting the Abu Darag Fault, which trends N57°W–S5757°E and spans most of the surveyed sites. Additionally, two other minor Tertiary faults—presumed to have originated during the Gulf of Suez (GOS) rifting phase—were identified at each site, except for Telal site which prompted further investigations. Their orientations were plotted onto the schmidt lower hemispheres that were produced earlier to establish correlation aimed to assess whether the Miocene GOS tectonics influenced the formation of the newly observed fracture sets. Their measured orientations are as follows:

- Tatweer Station: [N28°E–S28°W, NS]
- Banzeenah Station: [N72°E–S72°W, N48°W–S48°E]
- North Porto Station: [N128°E–S18°W, N37°E–S37°W]
- South Porto Station: [N33°W–S33°E, EW]
- Porto Station: [N46°E–S46°W, N13°W–S13°E]

4. Results

TENSOR PBT and right-dihedral analyses yielded rich information like the rose diagrams, Schmidt-Lower stereonet plots, best fitting mean stress axes

attitudes, mohr circle diagrams exclusive to each investigated site (Figure 5) (Figure 6).

In **S1-Tatweer site**, the local stress regime was transtension with extensional component in the direction of σ_{3-PBT} trending N115-N295 and/or $\sigma_{3-R,D}$ oriented N122-N302 as indicated by R-ratios where $R_{PBT} = 0.43$ and $R_{R,D} = 0.5$. In **S2-Banzeenah site**, the co-processing of both subsets proposed that ground had experienced non-pure axial extension oriented with $\sigma_{3-PBT} = N174-N354$ to $\sigma_{3-R,D} = \sigma_3 = N183-N003$ which was associated to the deduced tensor having ratios $R_{PBT} = 0.23$ and $R_{R,D} = 0.25$. In **S3-North Porto site**, two subsets were analyzed together to find the mean stress tensor which yielded axial extensional stress regime with σ_{3-PBT} axis oriented N76-N256 and $\sigma_{3-R,D}$ directed N75-N255 with $R_{PBT} = 0.25$ and $R_{R,D} = 0.5$. In **S4-South Porto site**, Same as previous, the simultaneous PBT and right-dihedral processing of two measured fracture subsets yielded a best fitting reduced tensor deduced pure extensional, R_{PBT} -ratio of 0.41 to transtension stress regime, $R_{R,D}$ -ratio of 0.62, oriented with σ_{3-PBT} directed N86-N266 and $\sigma_{3-R,D}$ directed N116-N296. Moreover, in **S5-Porto site**, the stress analysis yielded pure extensional stress regime, with associated $R_{PBT} = 0.48$ and $R_{R,D} = 0.5$ respectively, in the direction of $\sigma_{3-PBT} = \sigma_{3-R,D} = N143-N323$. Finally, in **S6-Telal site**, the previously mentioned analyses constructed a reduced tensor having the ratios $R_{PBT}, R_{R,D} = 0.5$ revealing an extensional regime in the direction $\sigma_{3-PBT} = \sigma_{3-R,D} = N23 - N203$.

Overlaying the Tertiary fault traces with neo-tectonic tensor results (Figure 7) reveals a dominant NNW-SSE with notable E-W orientations of the structural elements, suggesting the persistence of Miocene Gulf of Suez (GOS) rifting-related stress into the present day. Notable exceptions occur at Banzeenah and Porto, where ENE–WSW-oriented fractures were observed, indicating the influence of additional or localized tectonic forces that warrant further investigation.

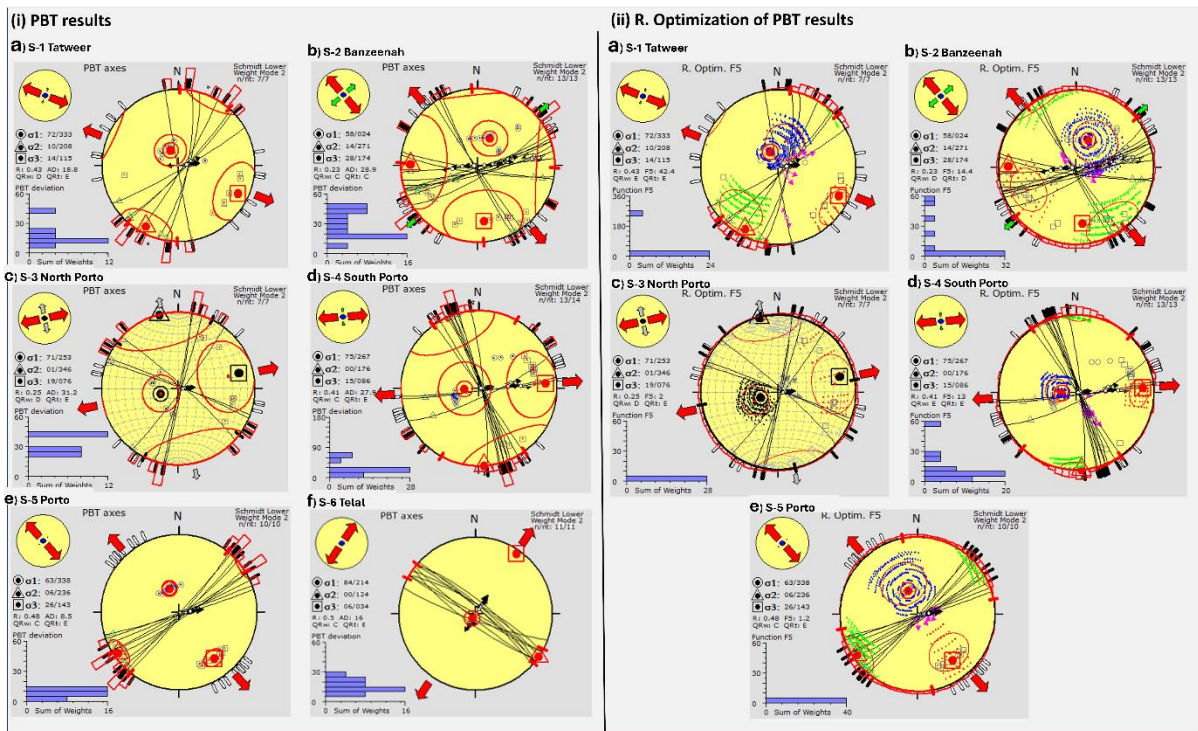


Fig.5. The results of the (i) PBT analysis and its (ii) right optimization showing the lower Schmidt hemisphere stereographic plots of the fractures found in a) S1-Tatweer, b) S2-Banzeenah, c) S3-North Porto, d) S4-South Porto, e) S5- Porto and f) S6-Telal sites. The theoretical shear deviations of each individual fracture is shown in the histogram on the lower left corner with the calculated deviation angles, which are the deviation of the predicted shear angle and the mean observed shear stress orientation (Delvaux et al., 1997), that is shown on y-axis and sum weights on x-axis which shows how homogenous the fault population is. The black arcs indicate the azimuths of the fracture's surfaces. . White circles with black and pink arrows indicate the slip vector for each fracture, black and pink colors of those small arrows only differentiate the slip vectors of the fractures categorized into two different subsets. The inward-pointing arrow indicates reverse slip, outward pointing arrow indicates a normal slip while double-opposing-half-headed arrows indicate strike slip. Black and white bars on the circumference of the stereonet indicate the axes of maximum horizontal stress axis (Shmax) and the minimum horizontal stress axis (Shmin) respectively for each individual fracture. Small circles, triangles and squares indicate the principal local stress axes plots for each individual fracture where (σ_1) is a blue dot inside a hollow black circle, (σ_2) is a green dot inside a hollow black triangle while (σ_3) is a red dot inside a hollow black square. Those axes are enclosed inside red ellipses or circles to point out the potential limits that encloses where the mean deviatoric stress axes will be plotted. Individual Red bold dots inside a big hollow red circles, triangle, square are the directions of the maximum principal stress (σ_1), the intermediate principal stress axis (σ_2) and the minimum stress axis (σ_3) respectively for the whole population. The direction of the deviatoric horizontal stress axes (Shmax) and (Shmin) are indicated by bold thick arrows on the upper left corner: Red outward pointing arrows indicate extensional regime while blue inward-pointing arrows indicate compressional stress regime, and their length and size indicate the magnitude of such stresses (Delvaux et al., 1997). In the same stress symbol on the upper left corner, the color of the middle dot indicates which principal stress axis is vertical (σ_v). . Either blue dot for (σ_1), green dot for (σ_2) or red dot for (σ_3). In the given symbol, the vertical stress axis is shown to be (σ_1) which indicates extensional stress regime.

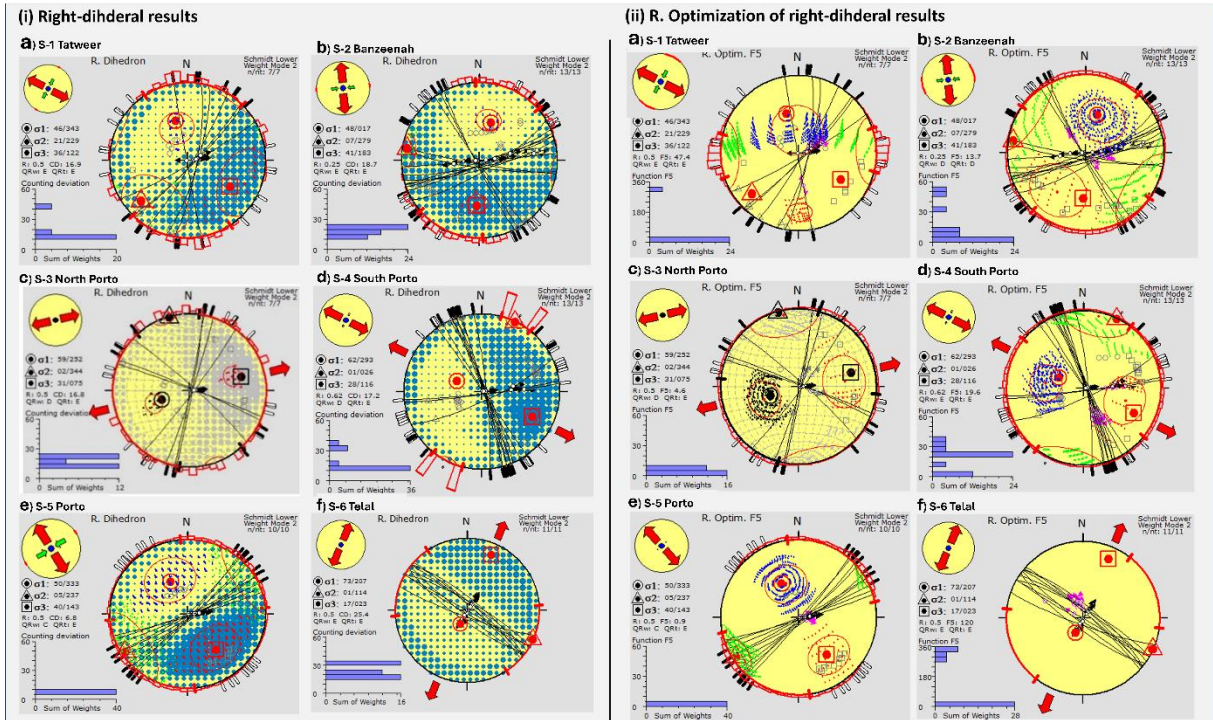


Fig. 6. The results of (i) the Right-dihedral analysis and (ii) its right optimization showing the lower Schmidt hemisphere stereographic plots of the fractures found in a) S1-Tatweer, b) S2-Banzeenah, c) S3-North Porto, d) S4-South Porto, e) S5- Porto and f) S6-Telal sites.

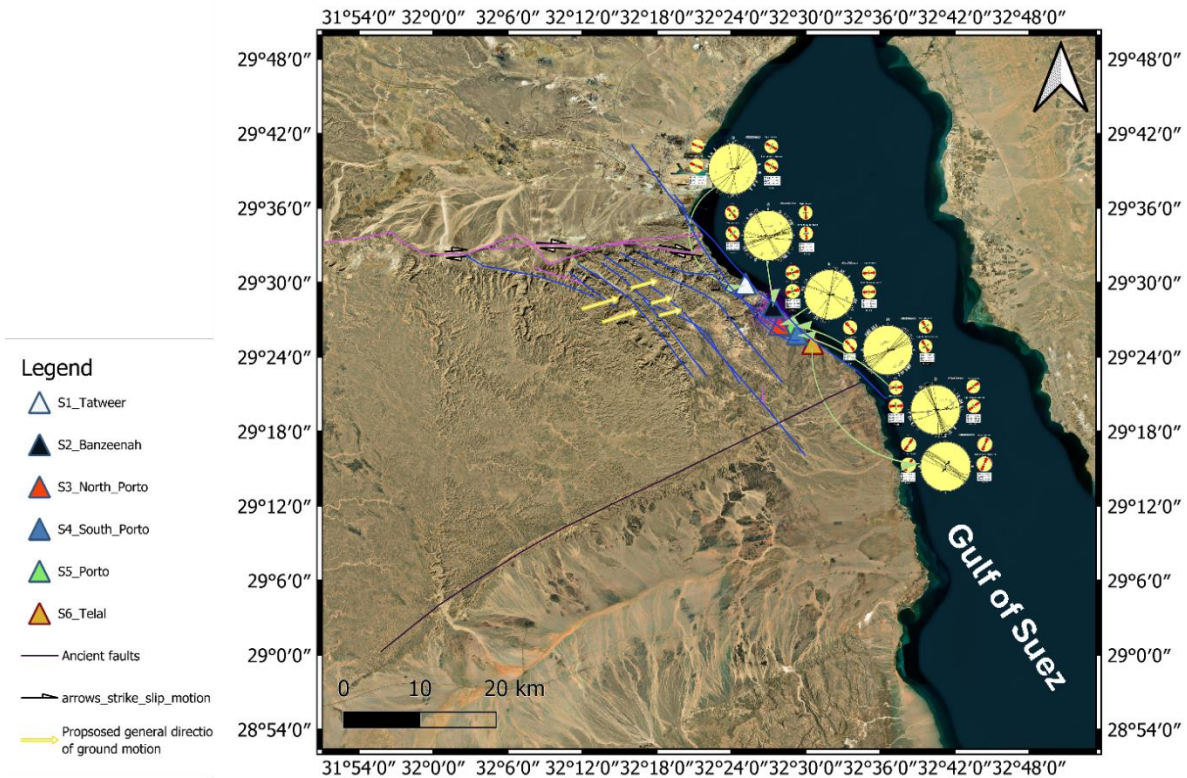


Fig. 7. Geospatial union between Tertiary fault sets line-vectors showing fault traces divided into three sets, set 1 shown in magenta-colored lines, set 2 marked as blue lines and set 3 colored in black, such traces were acquired from the work of (Khalaf et al., 2015), (Hussein and Abd-Allah, 2001). The floating plots of neotectonic tensor results such as the fractures Schmidt-lower stereonets projections and their responsible stress regime orientations where the red arrows symbolize σ_3 , for each site. The black half arrows indicate the strike slip component of the right-lateral diagonal slip movements forming the en echelon fault belts bounding the northern scarp of the plateau.

5. Discussion

The integration of major Tertiary fault traces with recent fracture-derived fault-plane solutions offers valuable insights into the potential mild reactivation of Tertiary rifting events in the present day. This geospatial correlation aids in identifying zones of ongoing tectonic activity and recognizing ancient faults that may remain active or have been reactivated. Using QGIS, the traceable ancient faults were digitally mapped, and stereonet projections along with corresponding stress field orientations were spatially overlaid. This allowed for the cartographic representation of local stress regimes inferred from neo-tectonic analyses at each site.

According to the previous literature, the Tertiary fault sets; Sets 1 and 2 were believed to have been reactivated by transtension stress regime (Moustafa and Abd-Allah, 1992) made up of right-lateral strike slip component and extensional component-oriented ENE-WSW (Figure 7). Such tectonic movement acted upon the pre-existing deep-seated E-W oriented normal faults causing them to propagate upwards in the form of en-echelon zig-zag normal fault belts.

Representative stress inversion results such as the Stress ratio, type of stress regime. Schmedit-Lower sterenet plots of the neo-tectonic PBT and right-dihedral analyses, along with the projected orientations of the Tertiary faults for S-1 Tatweer site are shown in (Figure 8) and (Figure 9) respectively. Also the Mohr circle representations from each analysis conducted to the fracture population the aforementioned sites are shown in (Figure 10) and (Figure 11) respectively while complete tensor results for all preexisting fault sets combined with the projections of the recent fractures discovered at the remaining investigated sites are presented in Appendix (A), Appendix (B). The interpreted general direction of ground displacement is towards the east as shown by yellow arrows in (Figure 7) since most of the traced faults across the Northern Galala Plateau and the western side of the Gulf of Suez had a normal sense of slip. Because their orientations and their triggering stress regime coincide with the mean stress regime of the investigated recent fractures.

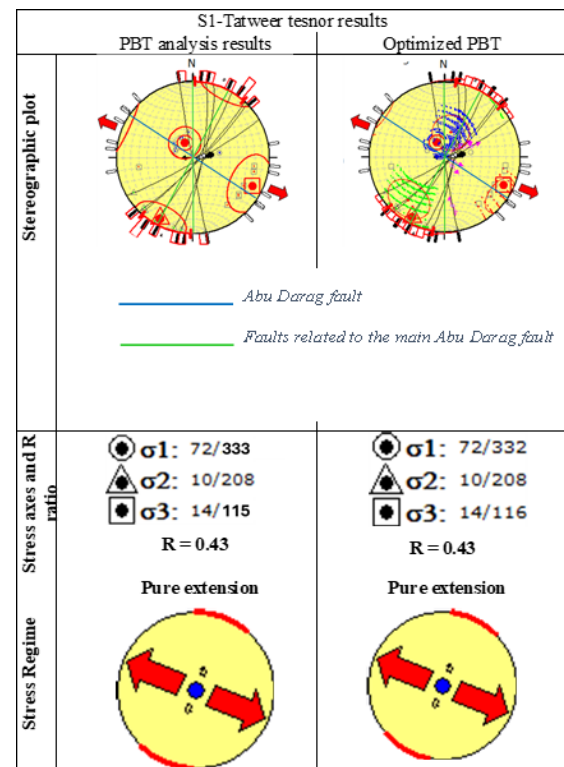


Fig.8. A compilation between the crucial products of TENSOR's PBT and optimized PBT analyses of the recent fractures with the orientations of some of ancient fractures discovered in S-1 Tatweer site

6. Conclusion

The study area was thoroughly examined prior to any analysis and is characterized primarily by mountainous terrain, interspersed with a few urbanized or metropolitan zones, which served as focal points for more detailed investigations. Historical and contemporary records confirm that the region has been tectonically and seismically active for centuries—likely since the onset of the Miocene African–Arabian plate divergence. This interpretation is supported by both previous studies and the results of the present neo-tectonic analysis, which identified the prevailing directions of extensional stress as a continuation of the ancient Red Sea–Gulf of Suez rifting event. Reactivation of NW–SE trending rift-related faults, along with pre-existing ancient structural features such as the Abu Darag Fault, appears to be a significant driver of modern seismicity across the plateau and more importantly across the areas under development along the western Gulf of Suez coasts. This

conclusion is reinforced by geospatial overlay analysis, which demonstrated a clear correlation between the trends and deriving tectonic forces of the ancient faults and the widely distributed recent surface fractures, implying that current tectonic forces are consistent with those active during the Miocene rifting phase. It's worth mentioning that the observed ongoing displacement along the Dead Sea–Gulf of Aqaba transform fault may have a distant trigger on the formation of some of the recently formed fractures. Overall, these findings indicate that the relatively flat terrains west of the Gulf of Suez are particularly susceptible to ground deformation, primarily due to their proximity to the divergent and transform plate boundaries.

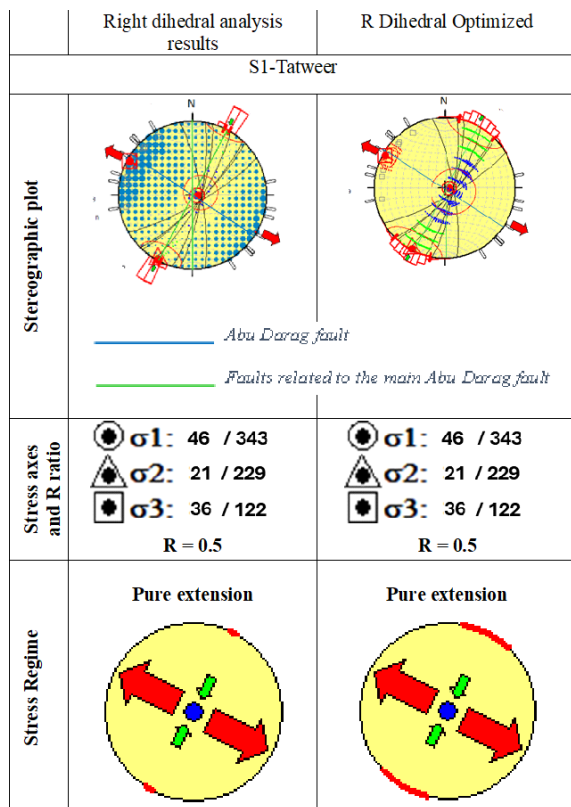


Fig. 9. An example of of compiled results of Right-dihedral analyses and their Right Optimization alongside the orientations of the measured pre-existing faults discovered in S-1 Tatweer site.

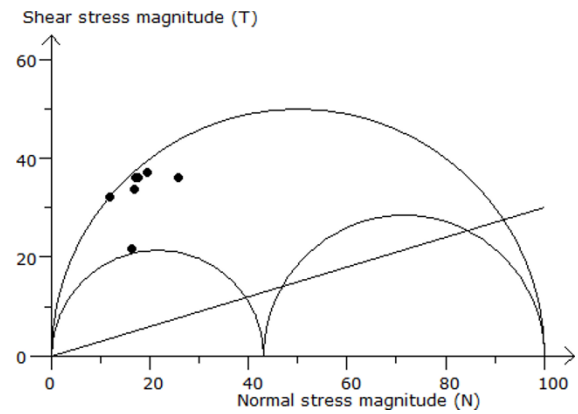


Fig. 10 The Mohr circle diagram resulted from the PBT analysis of the fracture population measured in S1-Tatweer site.

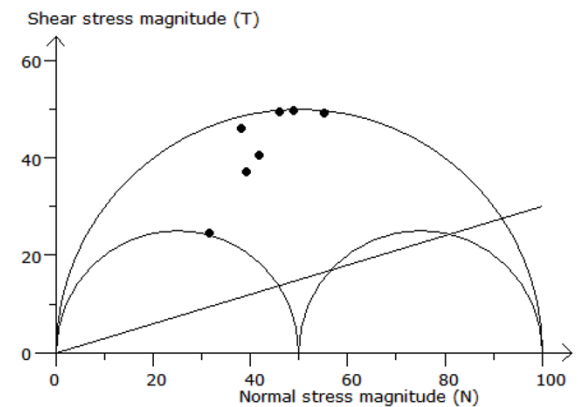


Fig. 11 The Mohr circle diagram resulted from the right-dihedral analysis of the fracture population measured in S1-Tatweer site.

Ethics approval and consent to participate: This article does not contain any studies with human participants or animals performed by any of the authors.

Consent for publication: All authors declare their consent for publication.

Conflicts of Interest: The author declares no conflict of interest.

Contribution of Authors: All authors shared in writing, editing and revising the MS and agree to its publication.

7. References

Abd-Allah, A. M. A. (1993). *Structural geology of the area between El Galala El Bahariya and Gebel Okheider*. Ain Shams.

Angelier, J. (1979). Determination of the mean principal directions of stresses for a given fault population. *Tectonophysics*, 56(3–4), [https://doi.org/10.1016/0040-1951\(79\)90081-7](https://doi.org/10.1016/0040-1951(79)90081-7)

Angelier, J. (1989). From orientation to magnitudes in paleostress determinations using fault slip data. *Journal of Structural Geology*, 11(1), 37–50.

- [https://doi.org/https://doi.org/10.1016/0191-8141\(89\)90034-5](https://doi.org/https://doi.org/10.1016/0191-8141(89)90034-5)
- Boukhary, M. A., Kenawy, A. I., & Basta, R. (2009). Early Eocene Nummulitids from Gebel Umm Russeies, El Galala El Bahariya, Eastern Desert, Egypt. *Geologia Croatica*, 62, 1–18.
- Delvaux, D. (1993). *The TENSOR program for paleostress reconstruction: examples from the east African and the Baikal rift zones*.
- Delvaux, D., Moeys, R., Stapel, G., Petit, C., Levi, K., Miroshnichenko, A., Ruzhich, V., & San'kov, V. (1997). Paleostress reconstructions and geodynamics of the Baikal region, Central Asia, Part 2. Cenozoic rifting. *Tectonophysics*, 282(1), 1–38. [https://doi.org/https://doi.org/10.1016/S0040-1951\(97\)00210-2](https://doi.org/https://doi.org/10.1016/S0040-1951(97)00210-2)
- Delvaux, D., & Sperner, B. (2003). New aspects of tectonic stress inversion with reference to the TENSOR program. *Geological Society, London, Special Publications*, 212, 75–100. <https://doi.org/10.1144/GSL.SP.2003.212.01.06>
- El Shinawi, A., Khedr, F., & Henaish, A. (2022). Hazard Assessment of Bedrock Discontinuities Using Integration of Structural Data and Geotechnical Characterization: A Case Study from the Northern Galala Plateau, Egypt. *Acta Montanistica Slovaca*, 27, 446–461. <https://doi.org/10.46544/AMS.v27i2.13>
- Farouk, S. (2015). Upper Cretaceous sequence stratigraphy of the Galala Plateaux, western side of the Gulf of Suez, Egypt. *Marine and Petroleum Geology*, 60, 136–158. <https://doi.org/https://doi.org/10.1016/j.marpetgeo.2014.11.005>
- Hussein, I. M., & Abd-Allah, A. (2001). Tectonic evolution of the northeastern part of the African continental margin, Egypt. *Journal of African Earth Sciences*, 33, 49–68. [https://doi.org/10.1016/S0899-5362\(01\)90090-9](https://doi.org/10.1016/S0899-5362(01)90090-9)
- Khalaf, E. A., Abdel Motelib, A., Hamed, M. S., & El Manawi, A. H. (2015). Volcano-sedimentary characteristics in the Abu Treifiya Basin, Cairo–Suez District, Egypt: Example of dynamics and fluidization over sedimentary and volcanoclastic beds by emplacement of syn-volcanic basaltic rocks. *Journal of Volcanology and Geothermal Research*, 308, 158–178. <https://doi.org/https://doi.org/10.1016/j.jvolgeores.2015.10.023>
- Khattari, K. (1973). Earthquake focal mechanism studies—A review. *Earth-Science Reviews*, 9(1), 19–63. [https://doi.org/https://doi.org/10.1016/0012-8252\(73\)90161-X](https://doi.org/https://doi.org/10.1016/0012-8252(73)90161-X)
- Lisle, R., Orife, T., & Arlegui, L. (2001). A stress inversion method requiring only fault slip sense. *Journal of Geophysical Research: Solid Earth*, 106. <https://doi.org/10.1029/2000JB900353>
- Mattila, J. (2015). *Genesis and evolution of brittle structures in southwestern Finland and western South Africa - insights into fault reactivation, fluid flow and structural maturity in Precambrian cratons*.
- McKenzie, D. (1969). The relation between fault plane solutions for earthquakes and the directions of the principal stresses. *Bulletin of the Seismological Society of America*, 59, 591–601. <https://api.semanticscholar.org/CorpusID:130069518>
- Moustafa, Adel. (2020). Mesozoic-Cenozoic Deformation History of Egypt. In Z. Hamimi, A. El-Barkooky, J. M. Frías, H. Fritz, & Y. A. El-Rahman (Eds.), *The Geology of Egypt* (1st ed., pp. 253–294). Springer Cham. https://doi.org/10.1007/978-3-030-15265-9_7
- Moustafa, A R, & Khalil, M. H. (1995). SUPERPOSED DEFORMATION IN THE NORTHERN SUEZ RIFT, EGYPT: RELEVANCE TO HYDROCARBONS EXPLORATION. *Journal of Petroleum Geology*, 18(3), 245–266. <https://doi.org/https://doi.org/10.1111/j.1747-5457.1995.tb00905.x>
- Moustafa, Adel R., & Abd-Allah, A. M. (1992). Transfer zones with en echelon faulting at the northern end of the Suez Rift. *Tectonics*, 11(3), 499–506. <https://doi.org/10.1029/91TC03184>
- Moustafa, Adel R, & Khalil, S. M. (2020). *Structural Setting and Tectonic Evolution of the Gulf of Suez, NW Red Sea and Gulf of Aqaba Rift Systems BT - The Geology of Egypt* (Z. Hamimi, A. El-Barkooky, J. Martínez Frías, H. Fritz, & Y. Abd El-Rahman (eds.); pp. 295–342). Springer International Publishing. https://doi.org/10.1007/978-3-030-15265-9_8
- Pollard, D. D., Saltzer, S. D., & Rubin, A. M. (1993). Stress inversion methods: are they based on faulty assumptions? *Journal of Structural Geology*, 15(8), 1045–1054. [https://doi.org/https://doi.org/10.1016/0191-8141\(93\)90176-B](https://doi.org/https://doi.org/10.1016/0191-8141(93)90176-B)
- Saada, S. A. (2016). Edge detection and depth estimation of Galala El Bahariya Plateau, Eastern Desert-Egypt, from aeromagnetic data. *Geomechanics and Geophysics for Geo-Energy and Geo-Resources*, 2(1), 25–41. <https://doi.org/10.1007/s40948-015-0019-6>
- Sawires, R., Peláez, J. A., Fat-Helbary, R. E., Ibrahim, H. A., & Hernández, M. T. G. (2015). An Updated Seismic Source Model for Egypt. In Abbas Moustafa (Ed.), *Earthquake Engineering - From Engineering Seismology to Optimal Seismic Design of Engineering Structures* (p. Ch. 1). IntechOpen. <https://doi.org/10.5772/58971>
- Sippel, J., Reicherter, K., & Mazur, S. (2007). Paleostress analysis applied to fault-slip data from the southern margin of the Central European Basin System. *DGMK/ÖGEW-Frühjahrstagung*, 9(1), 1–5.
- Younes, A. I., & McClay, K. (2002). Development of accommodation zones in the Gulf of Suez-Red Sea rift, Egypt. *AAPG Bulletin*, 86(6), 1003–1026.

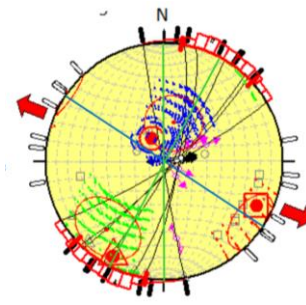
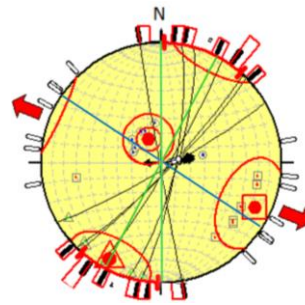
Appendix A: Detailed Tensor PBT Analysis Results

S1-Tatweer tensor results

PBT analysis results

Optimized PBT

Stress axes and Stereographic plot
R ratio



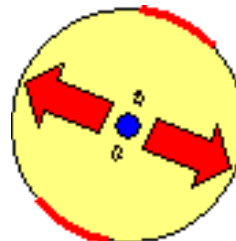
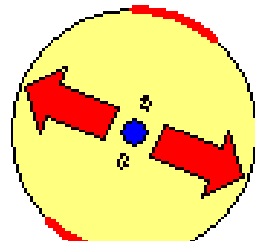
σ_1 : 72/333
 σ_2 : 10/208
 σ_3 : 14/115

σ_1 : 72/332
 σ_2 : 10/208
 σ_3 : 14/116

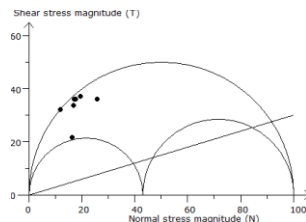
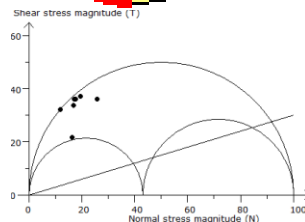
R = 0.43
Extension

R = 0.43
Extension

Stress Regime



Mohr Circle

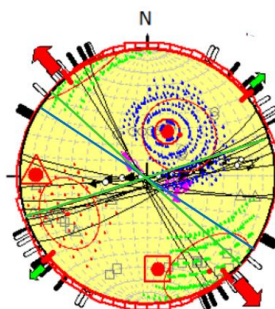
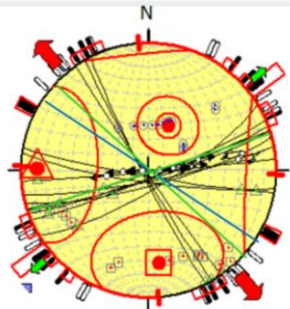


S2-Banzeenah tensor results (2 subsets)

PBT analysis results

Optimized PBT

Stereographic plot



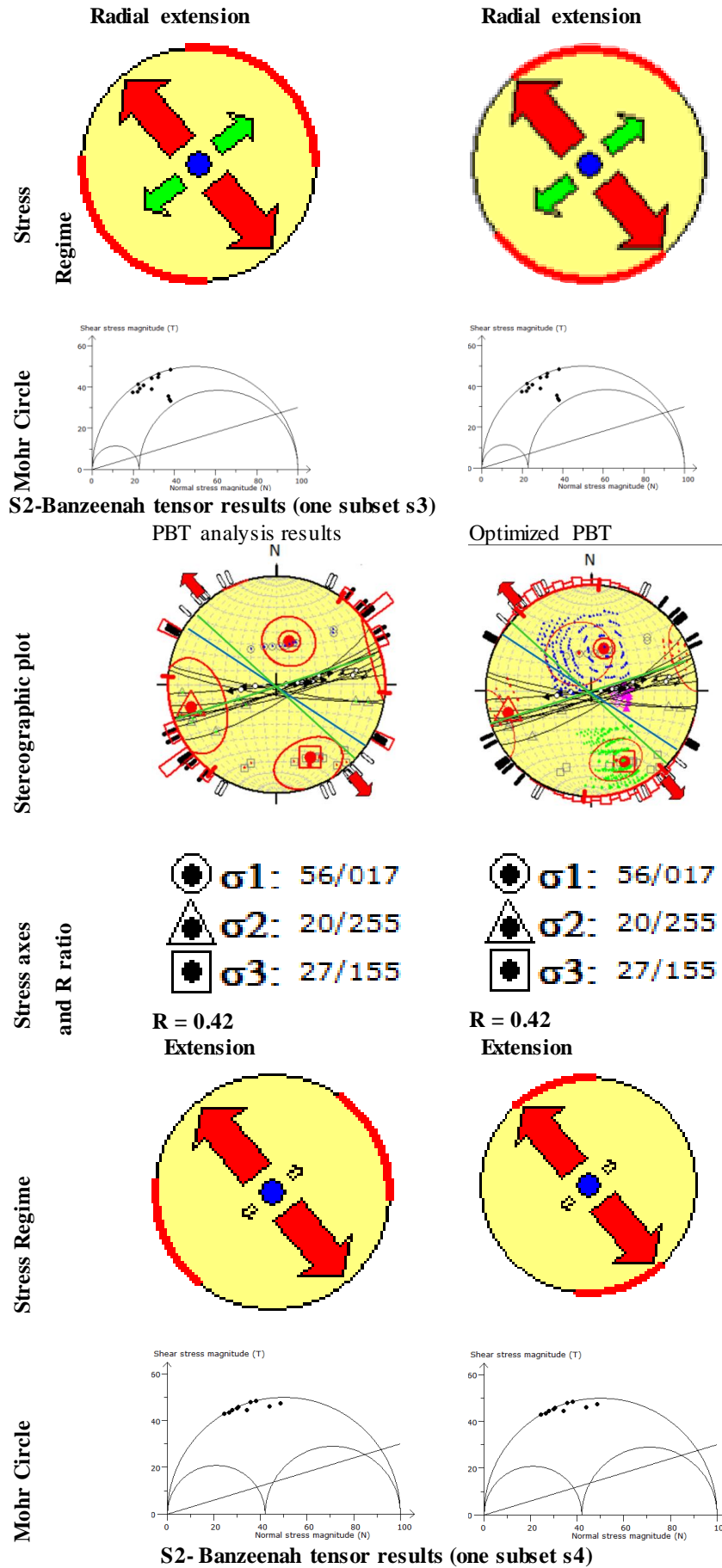
Stress axes and R ratio

σ_1 : 58/024
 σ_2 : 14/271
 σ_3 : 28/174

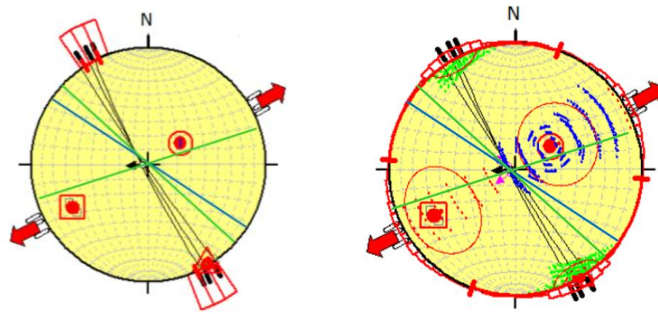
σ_1 : 58/024
 σ_2 : 14/271
 σ_3 : 28/174

R = 0.23

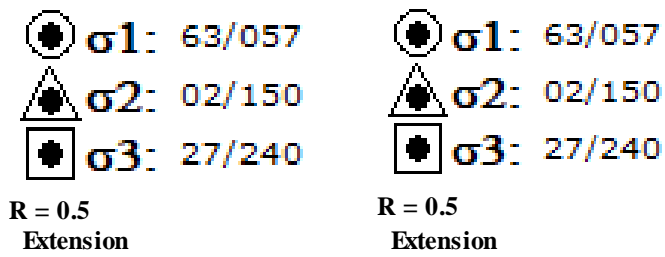
R = 0.23



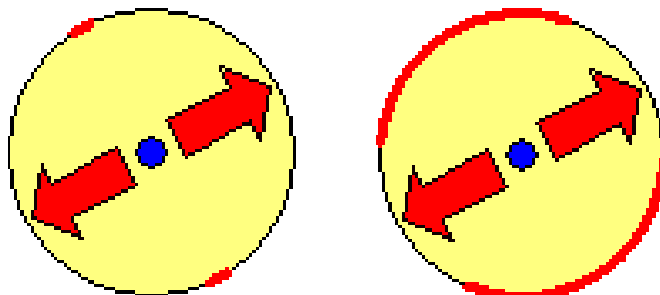
Stereographic plot



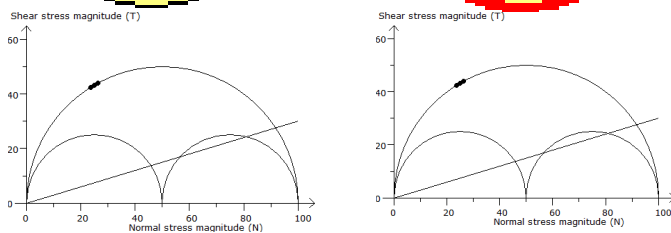
Stress axes and R ratio



Stress Regime



Mohr Circle

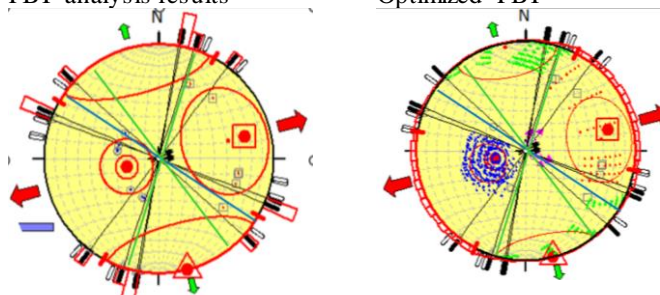


S3-North Porto tensor results (2 subsets)

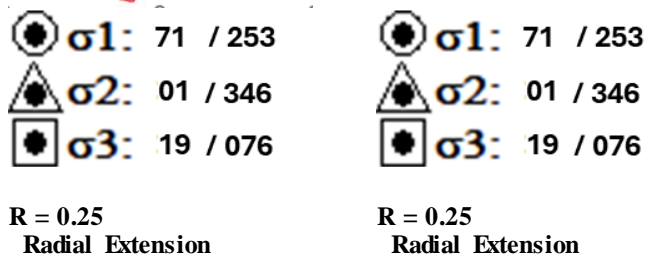
PBT analysis results

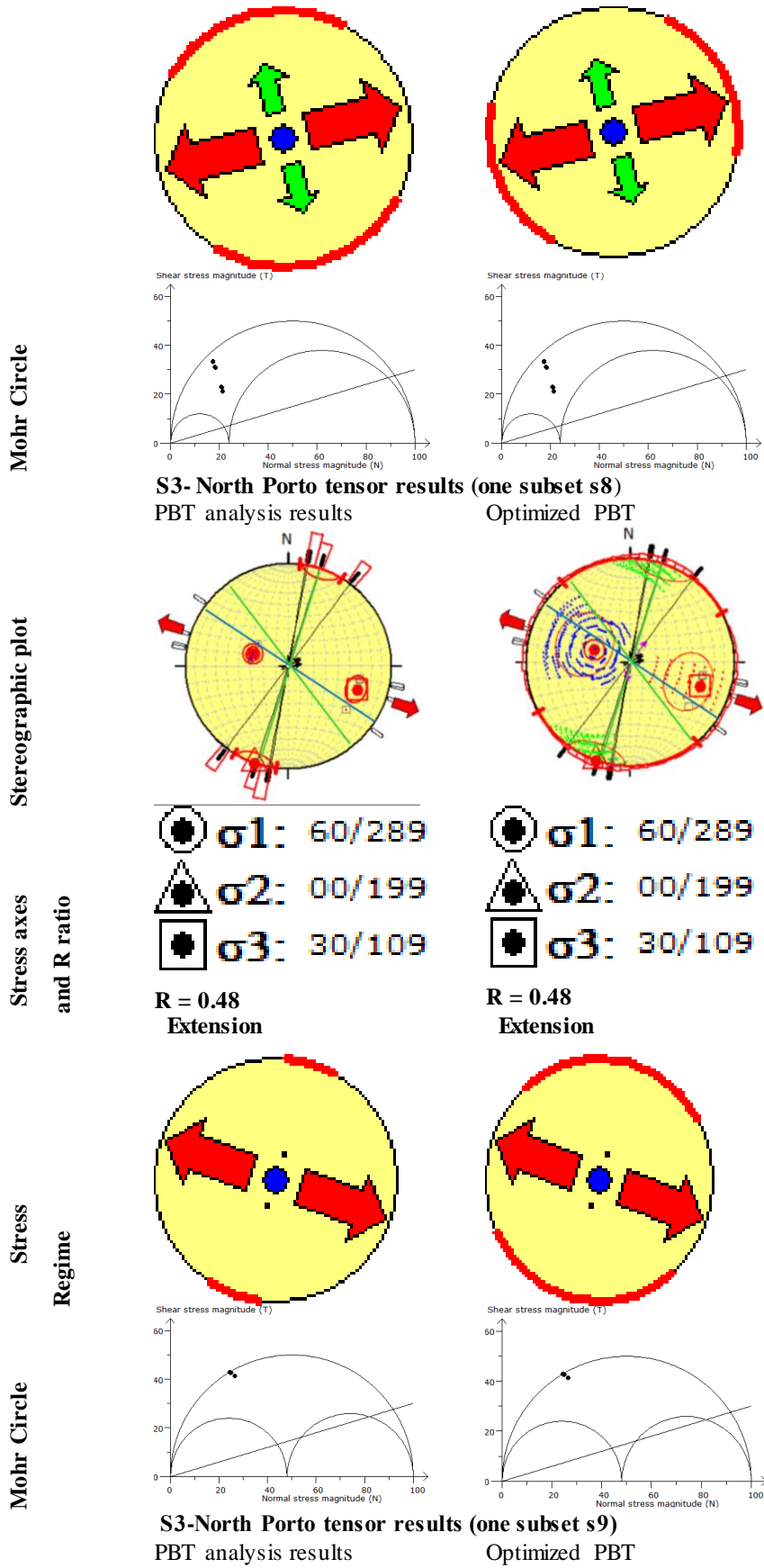
Optimized PBT

Stereographic plot

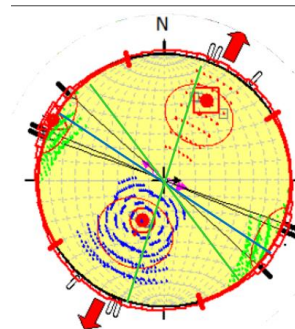
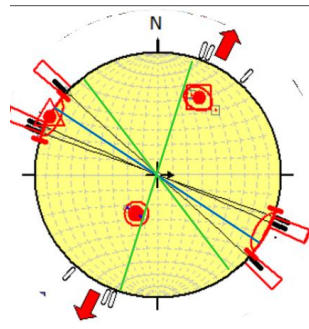


Stress axes and R ratio

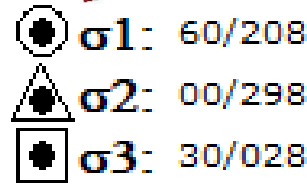
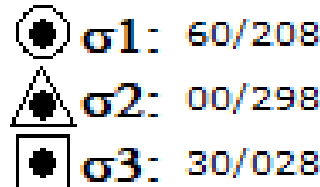




Stereographic plot



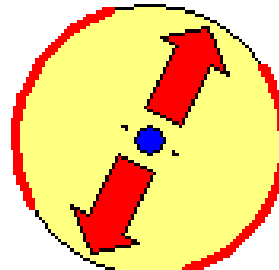
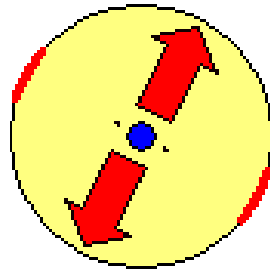
Stress axes
and R ratio



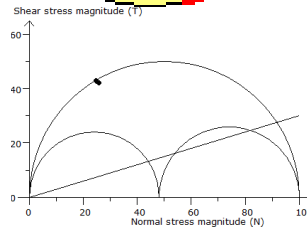
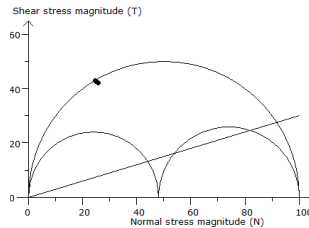
R = 0.48
Extension

R = 0.48
Extension

Stress
Regime



Mohr Circle

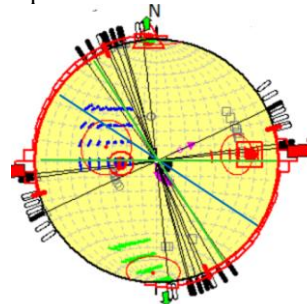
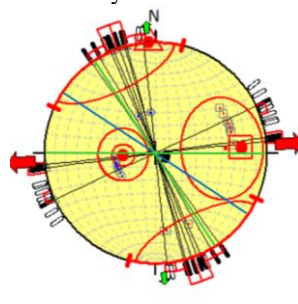


S4-South Porto Tensor results (2 subsets)

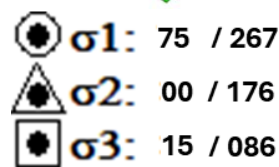
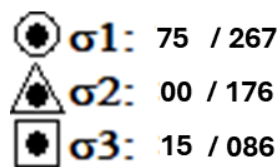
PBT analysis results

Optimized PBT

Stereographic plot

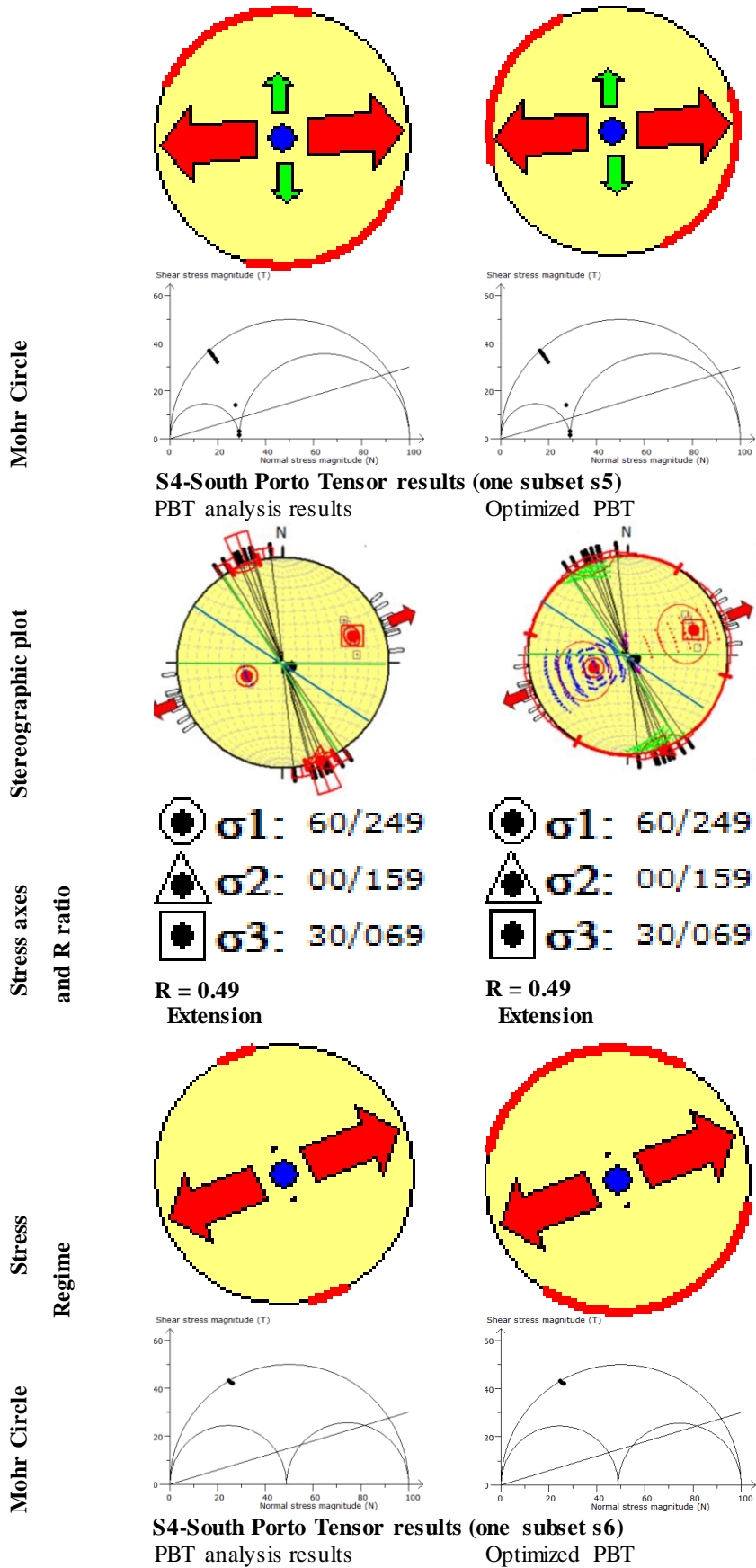


Stress axes
and R ratio

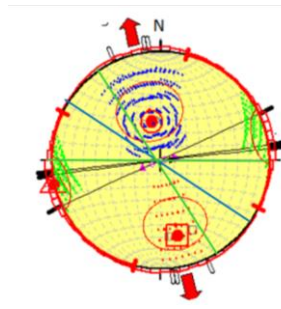
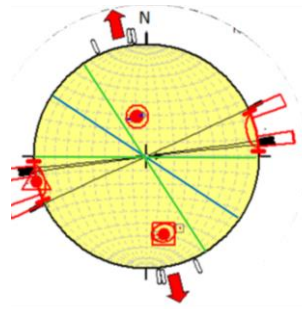


R = 0.41
Radial extension

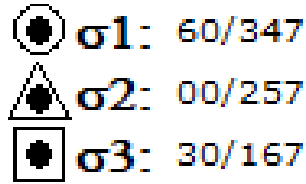
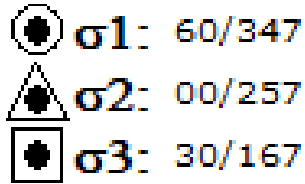
R = 0.41
Radial extension



Stereographic plot



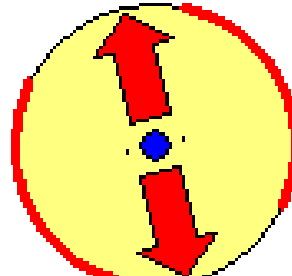
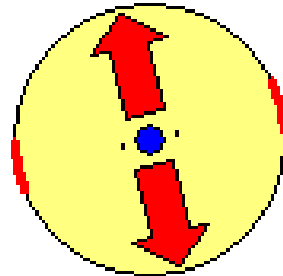
Stress axes
and R ratio



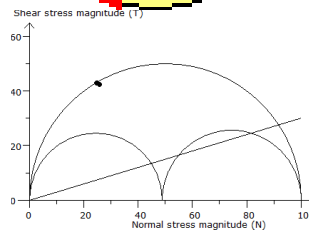
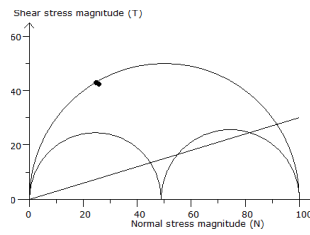
R = 0.49
Extension

R = 0.49
Extension

Stress
Regime



Mohr Circle

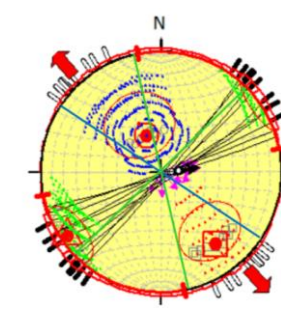
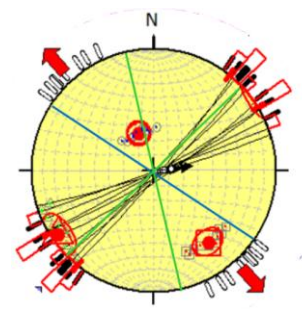


S5-Porto site tensor results

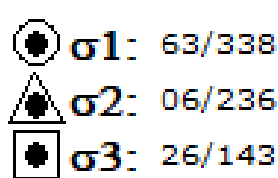
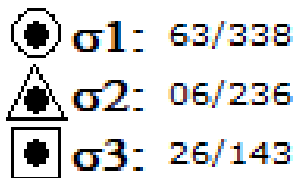
PBT analysis results

Optimized PBT

Stereographic plot

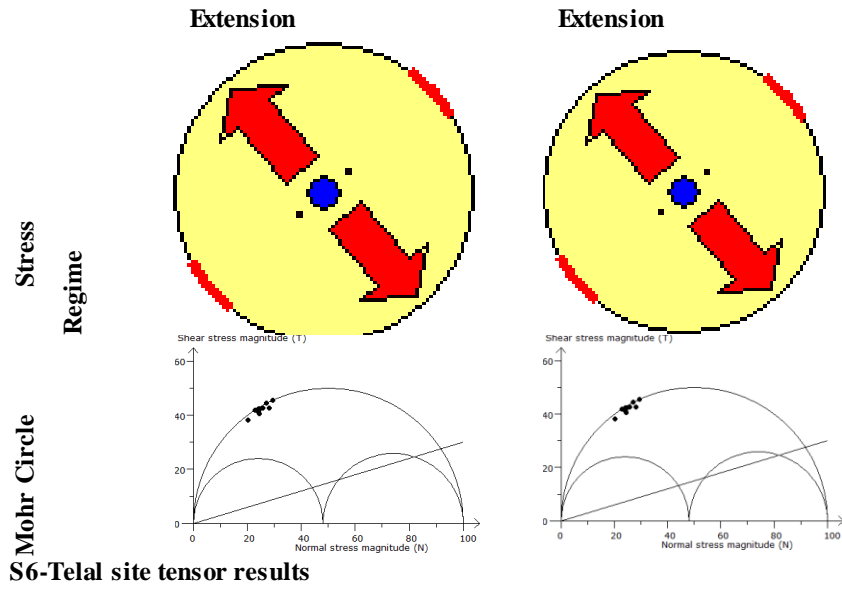


Stress axes
and R ratio

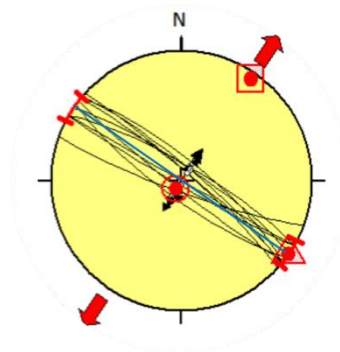


R = 0.48

R = 0.48



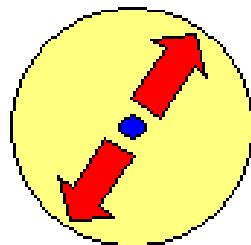
PBT results



- σ_1 : 84/214
- σ_2 : 00/124
- σ_3 : 06/034

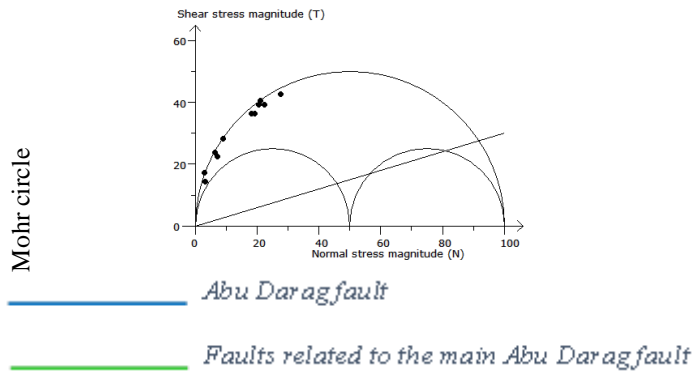
R = 0.5

Pure extension



Stress axes Stereonet plot and stress ratio

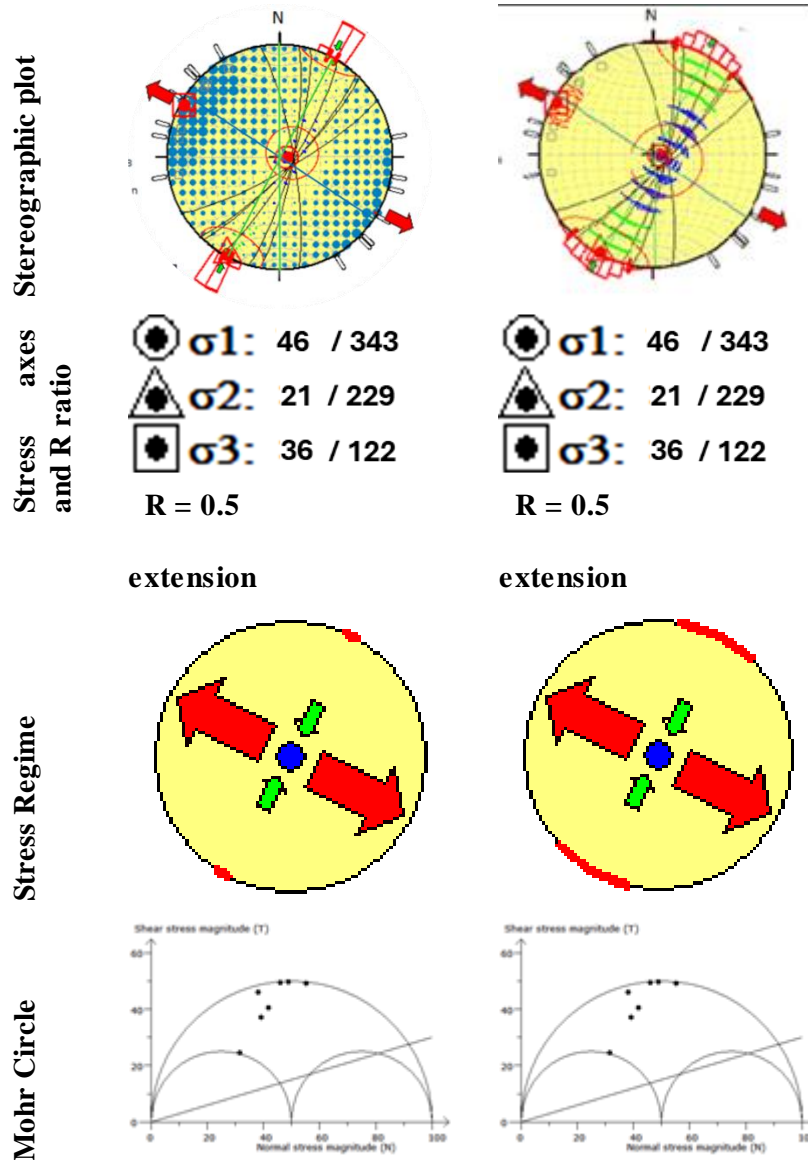
Stress regime



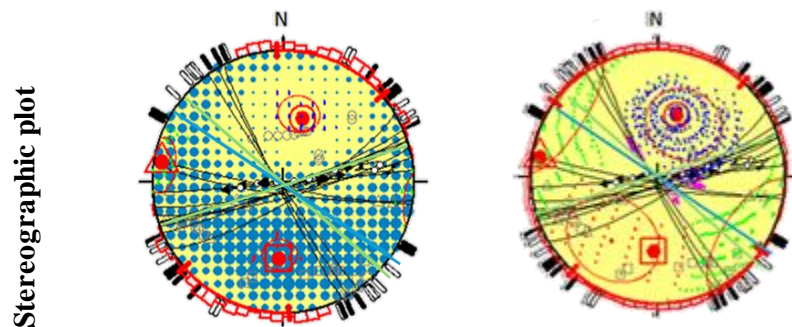
Appendix B: Detailed Tensor Right-dihedral Analysis Results

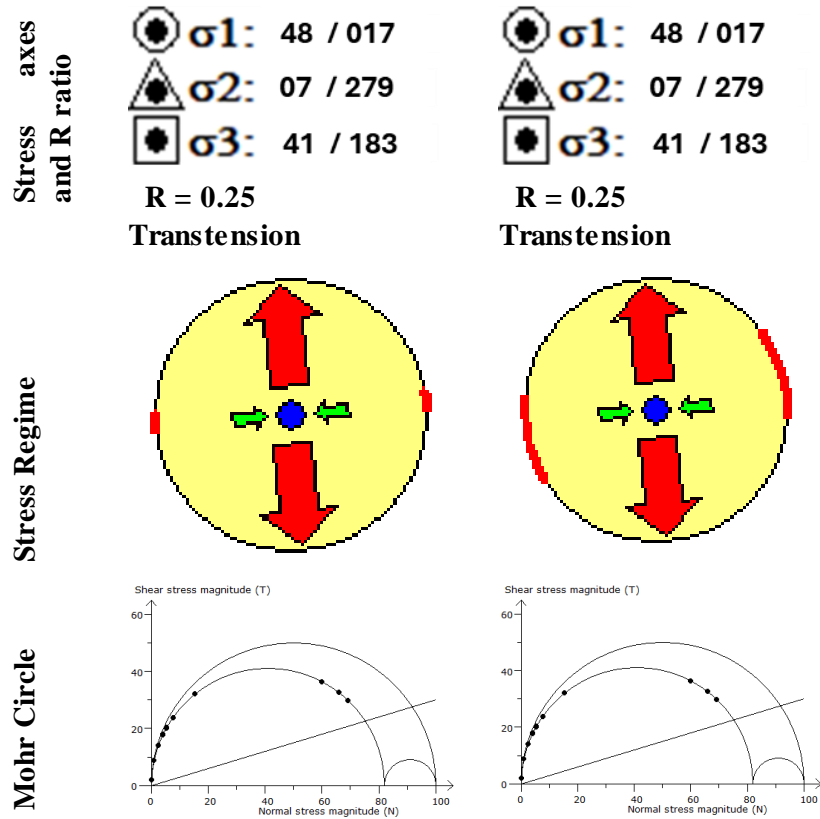
Right dihedral analysis R Dihedral Optimized results

S1-Tatweer

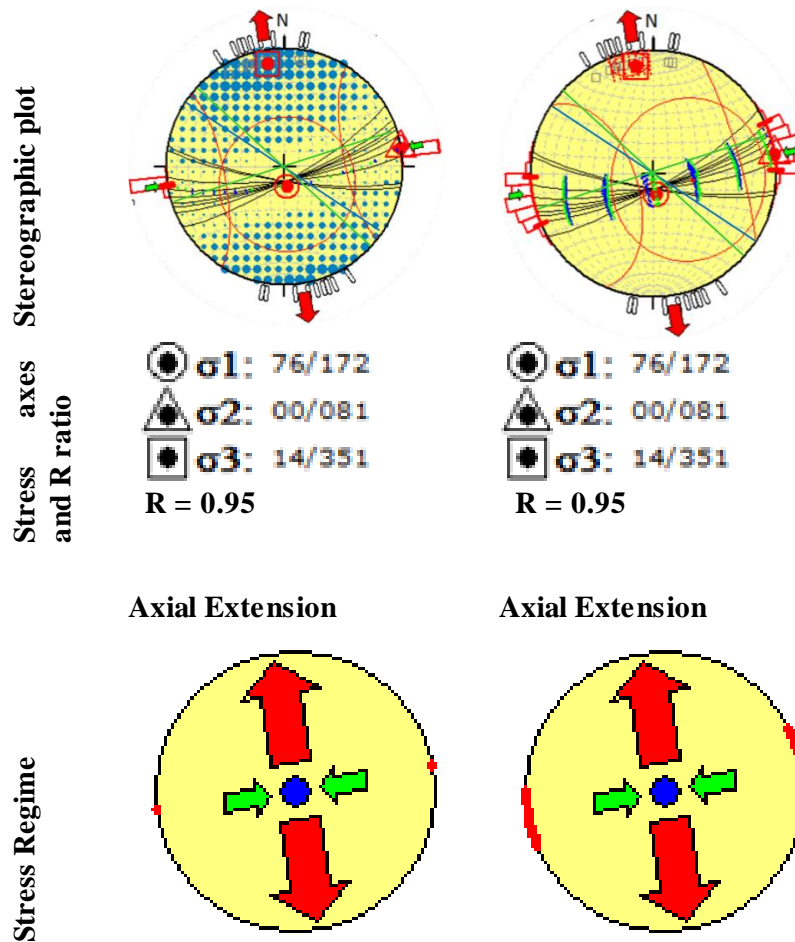


S2- Banzeenah (2 subsets)

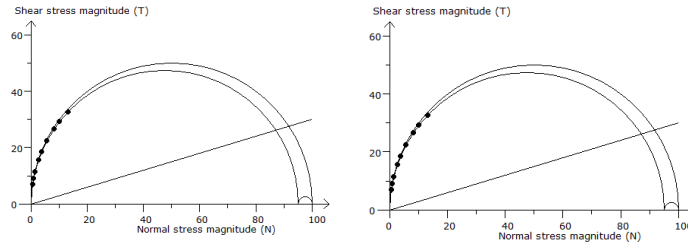




S2- Banzeenah tensor results (one subset s3)

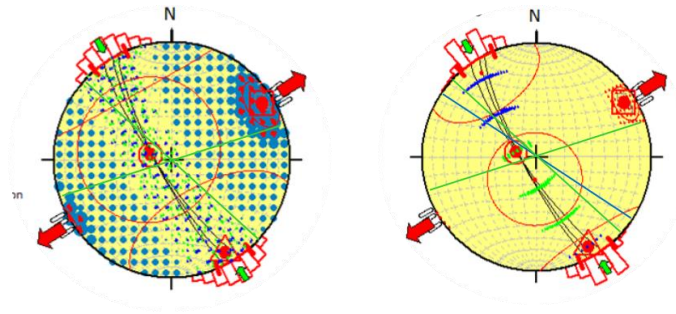


Mohr Circle

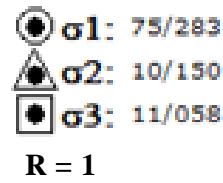
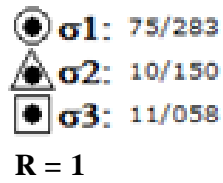


S2- Banzeenah tensor results (one subset s4)

Stereographic plot



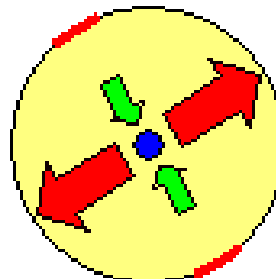
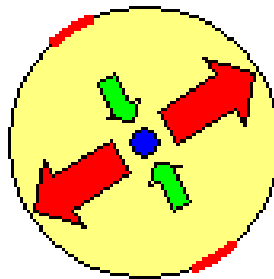
Stress axes and R ratio



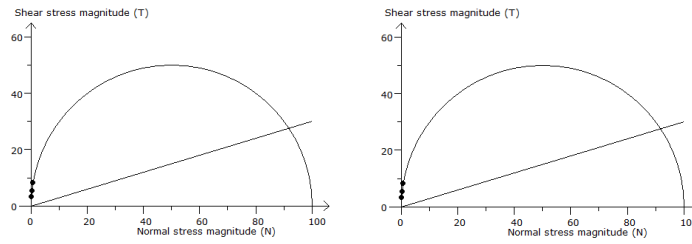
Stress Regime

Axial Extension

Axial Extension

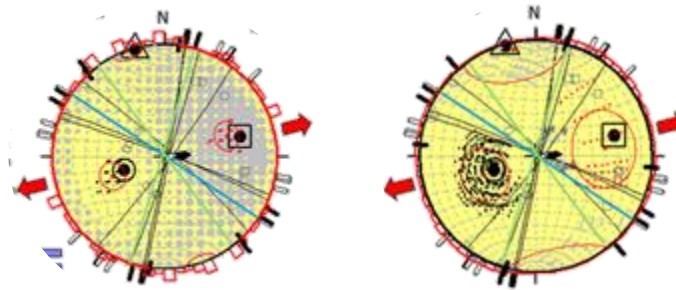


Mohr Circle



S3- North Porto tensor results (2 subsets)

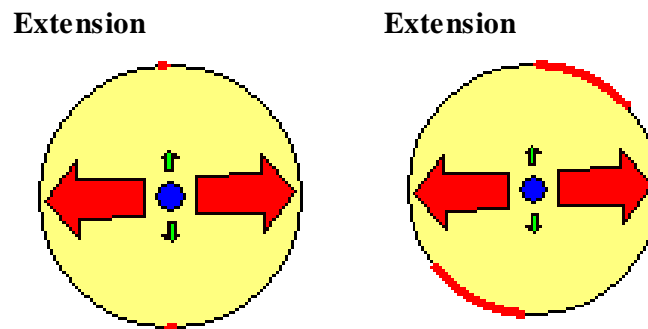
Stereographic plot



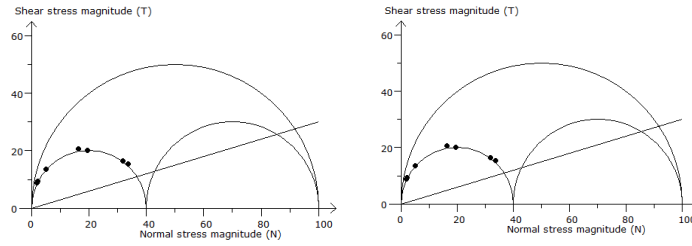
Stress axes and R ratio



Stress Regime

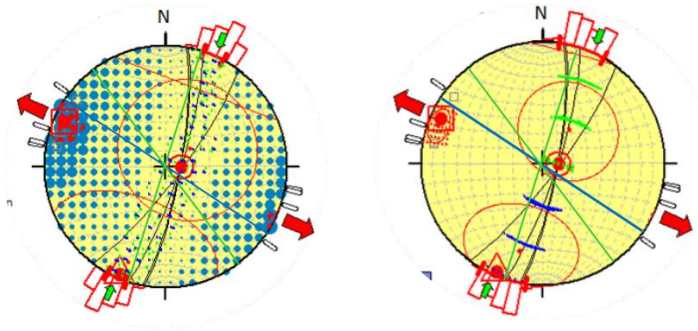


Mohr Circle

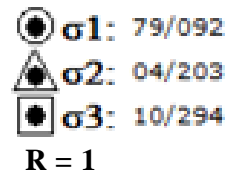
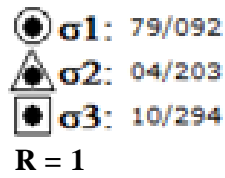


S3- North Porto tensor results (one subset s8)

Stereonet plot



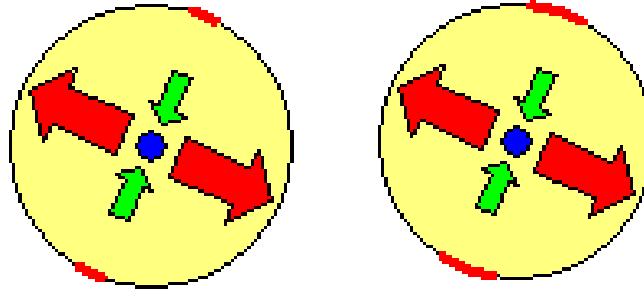
Stress axes and R ratio



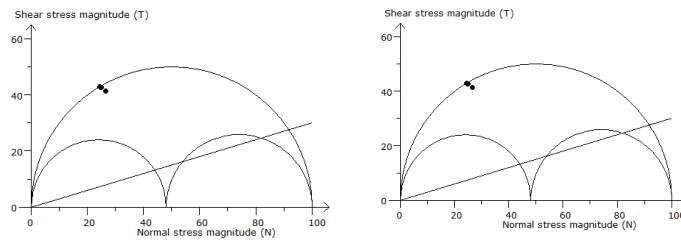
Axial Extension

Axial Extension

Stress Regime

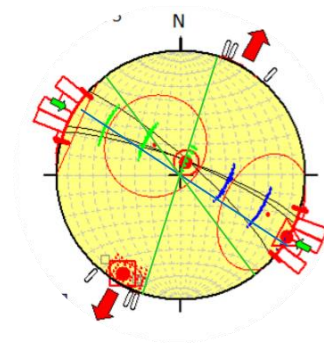
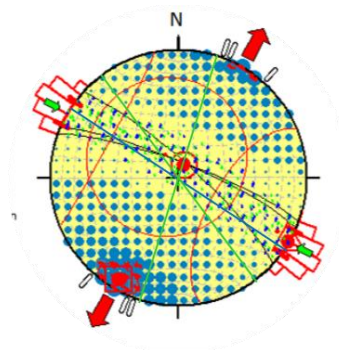


Mohr Circle



S3- North Porto tensor results (one subset s9)

Stereographic plot
Stress axes and
R ratio



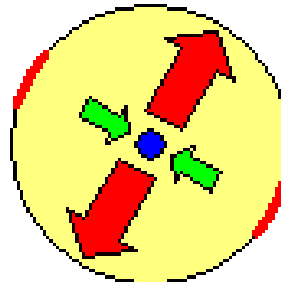
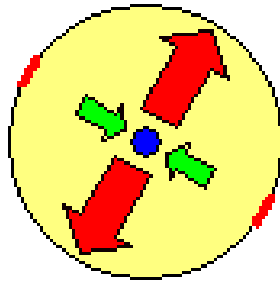
σ_1 : 81/025
 σ_2 : 01/120
 σ_3 : 09/210
R = 1

σ_1 : 81/025
 σ_2 : 01/120
 σ_3 : 09/210
R = 1

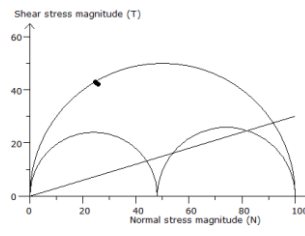
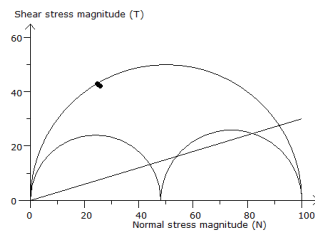
Stress Regime

Axial Extension

Axial Extension

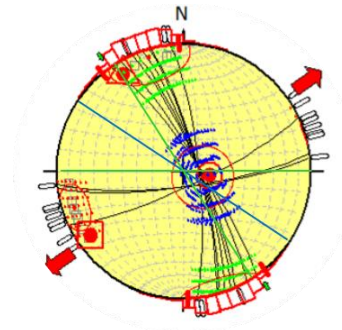
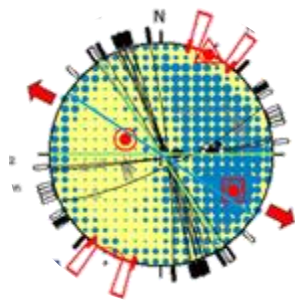


Mohr Circle

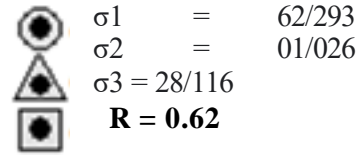
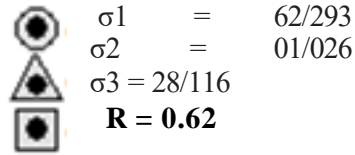


S4- South Porto Tensor results (2 subsets)

Stereonet plot



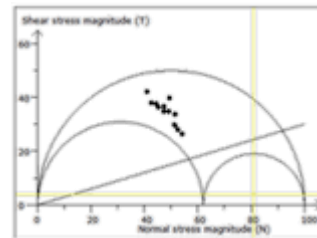
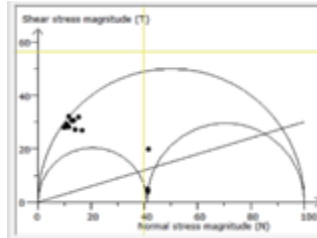
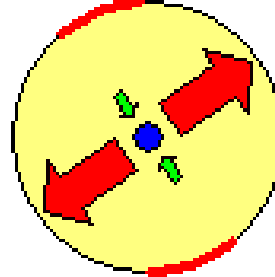
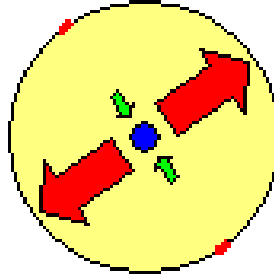
Stress axes
and R ratio



Transtension

Transtension

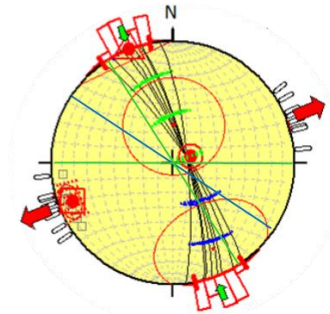
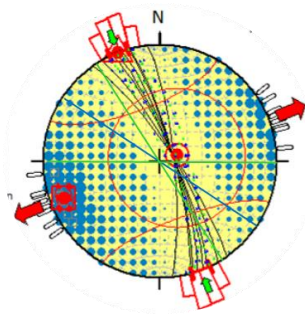
Stress Regime



Mohr Circle

S4- South Porto Tensor results (one subset s5)

Stereographic plot



Stress axes
and R ratio

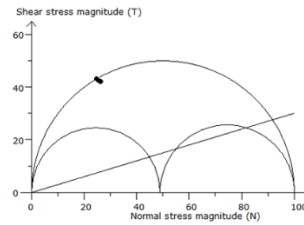
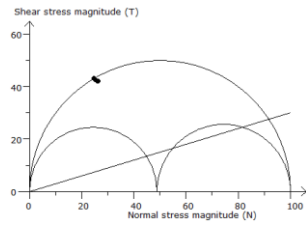
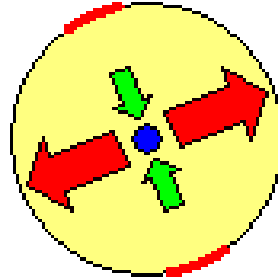
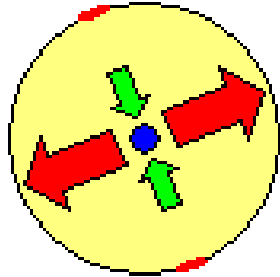
σ_1 : 77/071
 σ_2 : 00/339
 σ_3 : 13/249
 R = 1

σ_1 : 77/071
 σ_2 : 00/339
 σ_3 : 13/249
 R = 1

Axial Extension

Axial Extension

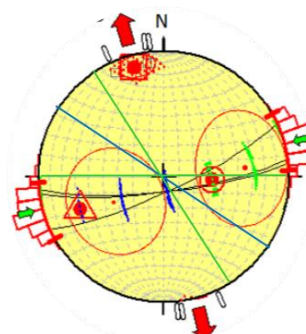
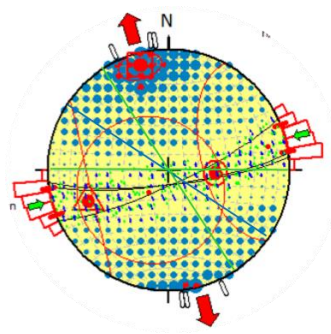
Stress Regime

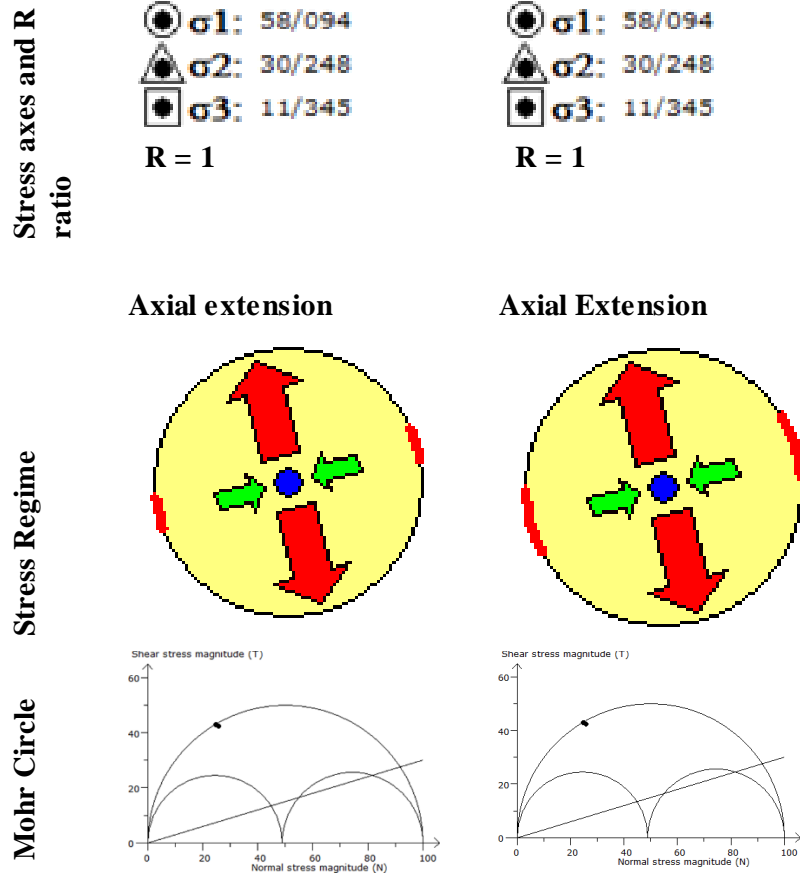


Mohr Circle

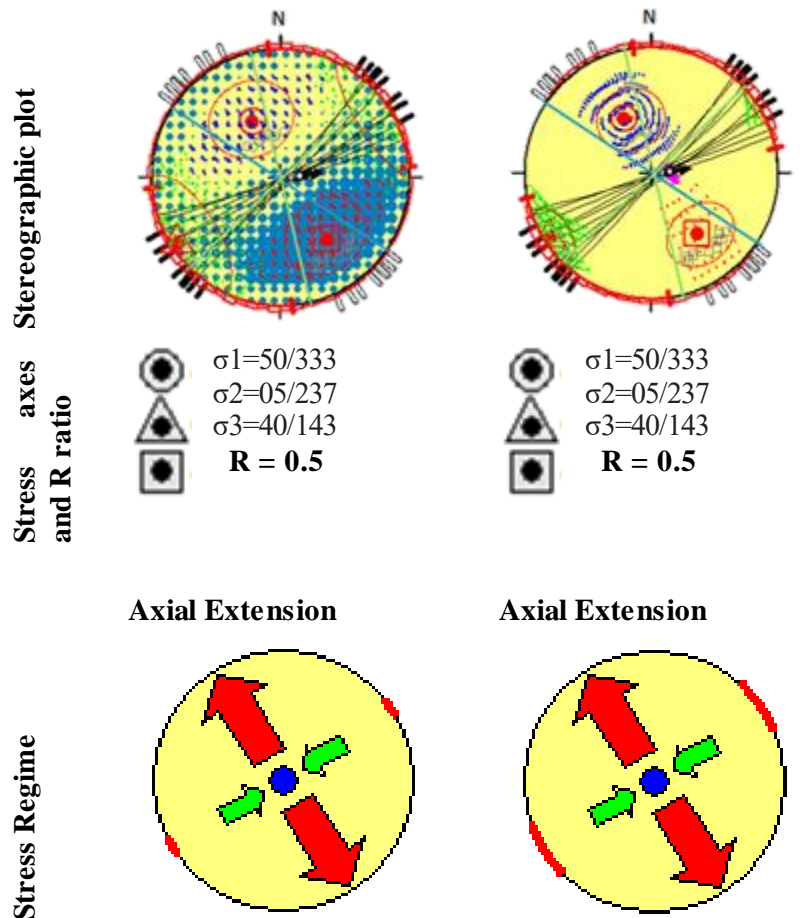
S4- South Porto Tensor results (one subset s6)

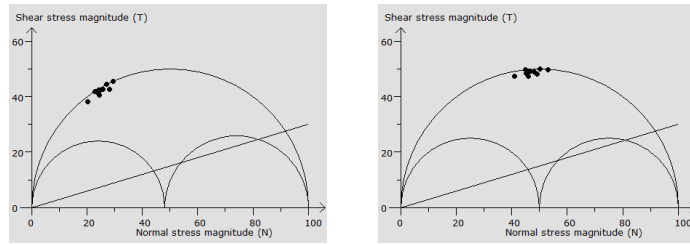
Stereonet plot





S5- Porto site tensor results

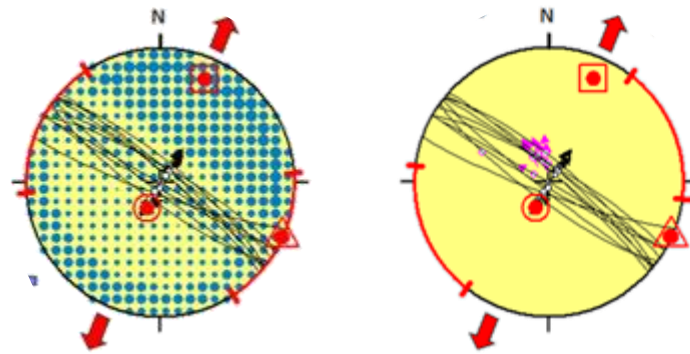




Mohr Circle

Telal site tensor results

Stereographic plot



Stress axes and R ratio

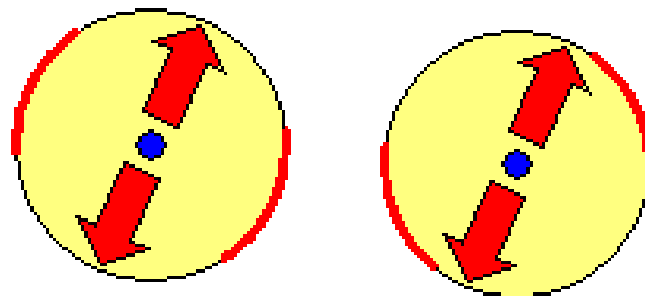
σ_1 : 73/207
 σ_2 : 01/114
 σ_3 : 17/023

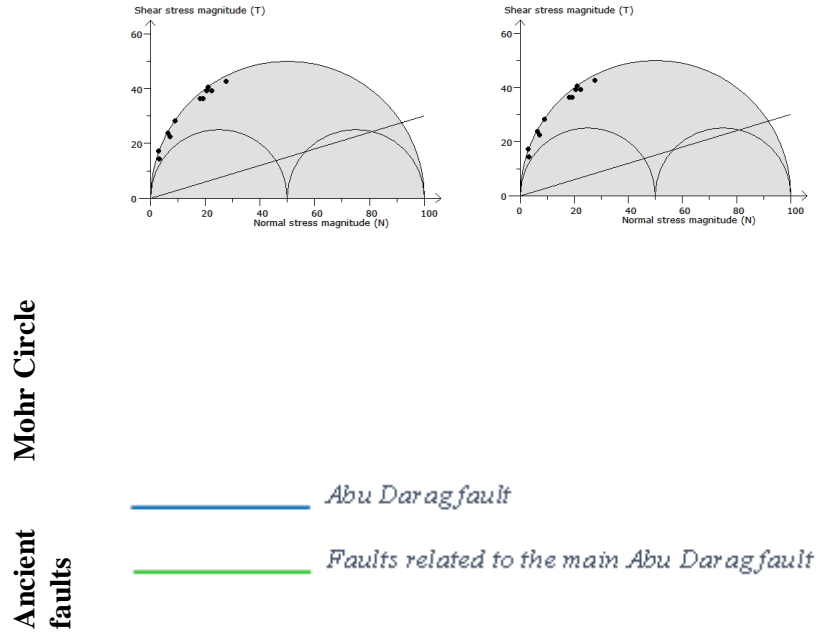
R = 0.5
Pure extension

σ_1 : 73/207
 σ_2 : 01/114
 σ_3 : 17/023

R = 0.5
Pure extension

Stress Regime





تقييم الاضطرابات الزلزالية الناجمة من أحد الصدوع الرئيسية للجانب الشمالي الغربي من أخدود خليج السويس بمصر

شادي عبد الهادي محمد^١، وكريم عبد الملك^١، وشريف محمد الهادي^٢، وعلي محمد علي عبد الله^١

^١ قسم الجيولوجيا، كلية العلوم، جامعة عين شمس، القاهرة، مصر

^٢ قسم الزلازل، المعهد القومي للبحوث الفلكية والجيوفيزيقية، حلوان، مصر

يشهد شمال غرب خليج السويس في مصر، نشاطاً تكتونياً مستمراً يُعتقد أنه امتداد للحركة التكتونية القديمة التي أدت تكون صدوع اخدود خليج السويس وهذا حتم اجراء دراسات تحليلية وتقييم مبدئي للانشطة الزلزالية المتكررة من الحركة على احد هذه الصدوع. ركزت الدراسة على عدد من المواقع الحضرية الواقعة على الساحل الغربي للخليج، حيث تم توثيق كسور أرضية حديثة وتحليلها ميدانياً بهدف فهم علاقتها بالنشاط الزلزالي الراهن. بدأت محاولات أولية في استخد تقنيات معكوس الإجهاد (TENSOR)، بما في ذلك طريقتا PBT و Right-Dihedral لتحليل بيانات الكسور المجمعة من ستة مواقع رئيسية. وأسفر التحليل عن نتائج متنوعة شملت تمثيلات اتجاهات محاور الاجهاد الرئيسية، وانشاء مخططات بيانية دائرية (Rose Diagram)، ودوائر موهر، وإسقاطات شبكات مجسمة (Stereographic projection)، أظهرت أنماط إجهاد محلية سمحت باستنتاج متوسط اتجاهات ونوع الاجهاد العام المؤثر على المنطقة ككل. أظهرت معظم المواقع اتجاهات إجهاد تسبب تمدد في القشرة الأرضية، في حين كُشف في بعض المواقع عن نظم إجهاد يجمع بين إزاحة أفقية ورأسية (transtensional) كما أظهرت المقارنة بين اتجاهات الكسور الحديثة مع الصدوع القديمة العميقة وجود تشابه في اتجاهات مضاربهم حيث وجد انه معظم الكسور تتخذ اتجاه متكرر الا وهو شمال شرق E-W و شمال-شمال-غرب جنوب-جنوب-شرق NNW-SSE، وهو ما يتماشى مع الاتجاهات محاور الاجهاد الرئيسية المرتبطة بالحركة التكتونية المسببة لفتح اخدود خليج السويس خلال العصر الميوسيني. يوجد استثناءات نجمت عن دراسة كسور منطقتي بنزينة وبورتو حيث وجدت الاتجاهات السائدة باتجاه شرق-شمال-شرقي غرب-جنوب-غرب (ENE-WSW)، مما يشير إلى وجود حركات تكتونية محلية إضافية تحيد عن الاتجاه العام للاجهاد المؤثر على منطقة شمال شرق مصر ككل. تؤكد هذه النتائج مجتمعة على أن بعض الفوالق القديمة ما زالت نشطة، وقد تكون بؤرة الانشطة الزلزالية المؤثرة على الحدود الغربية لخليج السويس.